

Resonant tunneling and the multichannel Kondo problem: the quantum Brownian motion description

Hangmo Yi

Department of Physics and Astronomy, University of Kentucky

Lexington, KY 40506-0055

(May 1, 2018)

We study mesoscopic resonant tunneling as well as multichannel Kondo problems by mapping them to a first-quantized quantum mechanical model of a particle moving in a multi-dimensional periodic potential with Ohmic dissipation. From a renormalization group analysis, we obtain phase diagrams of the quantum Brownian motion model with various lattice symmetries. For a symmorphic lattice, there are two phases at $T = 0$: a localized phase in which the particle is trapped in a potential minimum, and a free phase in which the particle is unaffected by the periodic potential. For a non-symmorphic lattice, however, there may be an additional intermediate phase in which the particle is neither localized nor completely free. The fixed point governing the intermediate phase is shown to be identical to the well-known multichannel Kondo fixed point in the Toulouse limit as well as the resonance fixed point of a quantum dot model and a double-barrier Luttinger liquid model. The mapping allows us to compute the fixed-point mobility μ^* of the quantum Brownian motion model exactly, using known conformal-field-theory results of the Kondo problem. From the mobility, we find that the peak value of the conductance resonance of a spin-1/2 quantum dot problem is given by $e^2/2h$. The scaling form of the resonance line shape is predicted.

PACS numbers: 05.40.+j, 05.30.-d, 72.15.Qm, 73.40.Gk

Contents

I	Introduction	2
II	Qualitative overview	3
III	Resonant tunneling of spinless electrons	6
IV	Multi-lead resonant tunneling models	8
V	Resonant tunneling in a Luttinger liquid	9
VI	General formalism of the QBM model	10
VII	Lattice models and phase diagrams	12
	A One-dimensional lattice	12
	B Triangular lattice and its D -dimensional generalization	13
	C Honeycomb lattice and its D -dimensional generalization	15
	D Distorted diamond lattice	17
	E Distorted honeycomb lattice: resonant tunneling of a spin-1/2 Luttinger liquid	18
VIII	Multichannel Kondo problem	18
IX	On-resonance conductance and the universal scaling	22
X	Conclusions	23
	APPENDIXES	23
A	Renormalization group analysis of the QBM model	23
B	Renormalization group analysis of the multichannel Kondo problem	25

1	Renormalization group flow equations	27
2	Fixed point mobility	28

I. INTRODUCTION

Electronic transport in mesoscopic systems has drawn much attention in the last decade due to recent development of fabrication techniques of ultra small structures of high quality. In the nanometer scale systems, electron-electron interactions play more important roles, as the number of effective spatial dimensions d is lowered. Most remarkable among many examples are fractional quantum Hall effect and Wigner crystallization at $d = 2$,¹ Luttinger liquid behavior at $d = 1$,²⁻⁴ and Coulomb blockade at $d = 0$.⁵ On the theoretical side, the use of traditional perturbative approaches were proven less useful due to the strong correlations, while nonperturbative techniques such as renormalization group, conformal field theory, and the Bethe ansatz have seen some success.

Studying resonant tunneling in a quantum dot coupled to leads via two identical quantum point contacts (QPC), Furusaki and Matveev⁶ showed that at $T = 0$, the on-resonance conductance of a spin-1/2 system takes a universal value less than the perfect conductance e^2/h .⁷ They argued that the on-resonance properties are controlled by the highly nontrivial non-Fermi-liquid fixed point of a four-channel Kondo problem. The deep connection between the problem of resonant tunneling in a point-contact-coupled quantum dot structure and the Kondo problem has been known for some time.^{8,9} A recent experiment¹⁰ has confirmed the theoretical predictions¹¹ of the capacitance line shape which was based on this connection.

Later, Yi and Kane¹² showed that there is a general and direct one-to-one mapping between the resonant tunneling problem and the Kondo problem in a special limit. They argued that this limit is a multichannel generalization of the well-known Toulouse limit.¹³ Using the conformal-field-theory results on the Kondo fixed point, they computed the universal conductance on resonance exactly.

They have also found that the quantum-field-theoretical formalism of both problems can be reduced to a first-quantized quantum mechanical formalism of a *fictitious* particle that moves in a periodic potential in a dissipative medium.¹⁴⁻¹⁶ Technically, this single-particle quantum Brownian motion (QBM) model is obtained by integrating out all degrees of freedom in the original quantum field theory except only a small finite number of them. These remaining degrees of freedom become the “spatial coordinates” of the Brownian particle and the integrated ones serve as the source of effective dissipation.

The symmetry of the periodic potential in the QBM model has been found to be crucial in identifying the zero-temperature phase diagram, while a particular phase is determined by the potential period and the dissipation strength. In particular, the on-resonance quantum dot problem were related to potentials with non-symmorphic lattice symmetries. A similar QBM model has been used in relatively recent studies in the context of resonance tunneling through an impurity state in a Luttinger liquid,^{17,18} which apply to such experimental situations as in quantum wires^{2,19} and quantum Hall edge systems.³ More applications of the QBM descriptions may also be found in connection with tunneling between quantum Hall edge states, both in fractional²⁰ and integer²¹ quantum Hall regime. A similar approach has also been used to study resonant point-contact tunneling between Luttinger-liquid leads,²² but the QBM model in that work was formulated with a π -flux through each plaquette.

In this paper, we extend the investigations in Ref. 12 and present a more general description of the QBM model as applied to (i) resonant tunneling in a quantum dot coupled to an arbitrary number of leads, (ii) multichannel Kondo problem, and (iii) resonant tunneling of Luttinger liquid through a double-barrier. As will be shown below, the QBM model possesses very rich phase diagrams. There are three zero-temperature phases: (i) the “free” phase in which the Brownian particle completely ignores the periodic potential, (ii) the “localized” phase in which the particle is trapped in a minimum of the periodic potential, (iii) and the most exotic of them all, the “intermediate” phase in which the particle is neither localized nor completely free. Each phase is characterized by a “mobility” μ — the ratio of the average velocity of the Brownian particle to the driving force in the linear response regime — which is universal in the sense that it is independent of the potential strength or other microscopic details. The mobility takes a perfect value in the free phase ($\mu = 1$), vanishes in the localized phase ($\mu = 0$), and takes a finite value between the two in the intermediate phase ($0 < \mu < 1$).

This paper is organized as follows. Sec. II is devoted to a general and qualitative overview of the QBM description of resonant tunneling and the multichannel Kondo problem. In Sec. III, we show how the one-dimensional (1D) QBM model is derived from the two-lead quantum dot model of spinless electrons and give a brief discussion on the universal scaling. We generalize this discussion to the multi-lead quantum dot model and the multichannel Kondo model in Sec. IV. Sec. V is devoted to the double-barrier resonant tunneling model of a Luttinger liquid. We discuss the similarities and differences between this model and the quantum dot model. In Sec. VI we develop a general

formalism of the QBM model and present the dual theories in the weak and strong backscattering limits. We define the mobility and introduce the renormalization group flow equation in both limits. In Sec. VII, we apply the QBM theory to specific lattice potentials. The zero-temperature phase diagram is derived for each lattice. It is also shown that there is a stable intermediate phase for non-symmorphic lattices. In Sec. VIII, we explicitly show that the QBM model is equivalent to the Toulouse limit of the multichannel Kondo model. We also show that the perturbation calculations of physically relevant quantities — the scaling dimension of the leading irrelevant operator and the fixed point mobility — are consistent with the exact solutions derived from conformal field theory results. In Sec. IX, we calculate the on-resonance conductance matrix G_{ab} of the multi-lead quantum dot model in terms of μ . Especially for the two-lead spin-1/2 problem, we calculate the conventional source-drain conductance G^* on resonance, as well as the scaling form of the resonance line shape. Finally, concluding remarks and discussions are given in Sec. X. Details of some lengthy calculations are given in appendices.

II. QUALITATIVE OVERVIEW

In this section, we will use a few simple examples to describe qualitatively the mapping between the QBM model, the resonant tunneling problem, and the multichannel Kondo problem. Rigorous derivations as well as more complicated systems will be discussed in the following sections.

The mapping between the QBM model and a mesoscopic tunneling problem is most easily understood by considering a single QPC formed by gates on a two-dimensional electron gas (2DEG), which is schematically depicted in Fig. 1. Experiments show that the linear conductance G through a QPC is quantized in units of e^2/h ,^{23–25} which is a characteristic signature of non-interacting 1D electron systems.²⁶ Indeed, a QPC may be thought of as a wave guide of an electron wave function, and each wave mode plays the role of a 1D channel. Each fully transmitting 1D channel contributes one conductance quantum e^2/h to the total conductance of a QPC.²⁷

As explained below, it is possible to see how a QPC is described by a QBM model, without going into too much detail. As the first example, we will consider a QPC that fully transmits only one 1D channel and we will construct a QBM model that reproduces the correct quantized conductance. The current is obviously given by $I = -e\partial_t Q$, where Q is the number of electrons in the source 2DEG lead. The Euclidean action may be written as

$$S = S_0 + S_{\text{source}}, \quad (2.1)$$

where S_0 is the unperturbed action, and S_{source} is the source term due to voltage drop V across the QPC. The second term is straightforwardly given from electrostatics by

$$S_{\text{source}} = - \int d\tau e Q(\tau) V, \quad (2.2)$$

where $\tau = it$ is the imaginary time. Using the Kubo formula, the linear conductance is written as

$$G = \lim_{V \rightarrow 0} \frac{\partial}{\partial V} \langle I \rangle \quad (2.3)$$

$$= \lim_{\omega \rightarrow 0} \frac{1}{\hbar|\omega|} \int d\tau e^{i\omega\tau} \langle T_\tau I(\tau) I(0) \rangle \quad (2.4)$$

$$= \lim_{\omega \rightarrow 0} \frac{e^2}{h|\omega|} \int d\omega' \omega \omega' \langle Q(\omega) Q(-\omega') \rangle. \quad (2.5)$$

If we assume that S_0 has a simple quadratic form and the Hamiltonian does not explicitly depend on time, then it *must* have the following form in order to yield the correct quantized conductance:

$$S_0 = \frac{1}{2} \int d\omega |\omega| |Q(\omega)|^2. \quad (2.6)$$

This may be thought of as an action of a QBM model written in terms of the spatial coordinate of the Brownian particle, Q .

A rigorous derivation of the action using the bosonization method²⁸ reveals that the above supposition is correct. In the boson representation, a generic non-interacting free 1D electron system is described by a Euclidean action^{29,17}

$$S_B = \frac{1}{8\pi v_F} \int d\tau dx [(\partial_\tau \theta)^2 + (v_F \partial_x \theta)^2], \quad (2.7)$$

where v_F is the Fermi velocity. The boson field $\theta(x, \tau)$ may be thought of as the local phase of a 1D charge density wave. Especially, it satisfies $\partial_t \theta = 2\pi I$ and $\partial_x \theta = 2\pi \rho$, where I is the current and ρ is the number density of electrons. If we define the coordinate system such that $x = 0$ at the center of the QPC, then

$$Q(t) = \int_0^\infty dx \rho(x, t) \quad (2.8)$$

$$= -\frac{\theta(x=0, t)}{2\pi} + \text{const.} \quad (2.9)$$

Integrating out $\theta(x, \tau)$ except for $x = 0$, one can easily see that the effective action is indeed given by Eq. (2.6).

Note that the non-analytic form of S_0 suggests that the Brownian particle is not free. This is due to the dissipation provided by $\theta(x \neq 0)$ after they are integrated out. The analogy between the QPC problem and the QBM model is completed by mapping the current I to the average “final velocity” of the Brownian particle and the voltage drop V to the “uniform external force”. The dissipation is indeed necessary to prevent $\partial_t Q$ from increasing indefinitely, because we know from the Ohm’s law that it is finite. Even though the QBM action may have to be modified for more complicated systems, the above mappings of fundamental quantities are universal.

Let us now include backscattering by pinching off the point contact via gate voltage. It is equivalent to placing a backscattering barrier at the center of the QPC that suppresses electron tunneling. If the barrier is strong, tunneling is almost suppressed and Q is strongly quantized at integers due to the discrete nature of electron number. On the other hand, if the barrier is weak, Q is only weakly quantized. However, as long as the barrier strength is nonzero, quantization effect is also nonzero. This effect is most simply taken into account by adding a term periodic in Q to the action. Since the period is one, the most generic backscattering action takes the form

$$S_v = -\sum_{n=1}^{\infty} \int \frac{d\tau}{\tau_c} \left[v_n e^{i2\pi n Q(\tau)} + \text{c.c.} \right], \quad (2.10)$$

where v_n is a dimensionless backscattering amplitude and τ_c is a short-time cutoff. In the QBM model, this describes a periodic potential. The potential gets tilted if the external uniform force term S_{source} in Eq. (2.2) is also added. This is schematically illustrated in Fig. 2. Transferring an electron across the point contact corresponds to moving the fictitious Brownian particle from a minimum of the potential to the next minimum. If we define the “mobility” of the particle μ as the final velocity $\langle \partial_t Q \rangle$ divided by the external force eV in the linear response regime, it is obviously the same as the electric conductance G up to a constant factor e^2 .

If the barrier is strong, it is more convenient to think of the QPC system as two almost separate leads that are weakly coupled by a small tunneling amplitude t . The corresponding QBM model is described by hopping of the Brownian particle between “lattice sites” that lie on deep minima of the periodic potential. In the above example, the lattice is a simple 1D lattice with lattice constant $a = 1$.

Another example in which the 1D QBM description is useful is the interacting 1D electron system known as Luttinger liquid. Again, if we focus on the current past a certain reference point, say $x = 0$, we may obtain a QBM model by integrating out all degrees of freedom except Q , which is again defined as the total number of electrons on the positive axis ($x > 0$). If there is a backscattering center such as a point impurity at $x = 0$, it gives rise to a periodic potential in the QBM model. The resulting total action is analogous to Eqs. (2.6) and (2.10), but the Luttinger-liquid correlation modifies the coefficient in front of S_0 which characterizes dissipation. Since we can restore the coefficient $1/2$ in Eq. (2.6) by rescaling Q , it may be alternatively said that the Luttinger liquid correlation modifies the period of the potential. From this point on, we will adopt the convention in which the dissipation coefficient is fixed at $1/2$ whereas the period a is a variable.

The 1D QBM model was studied over a decade ago in quite a different context, namely, as a possible description of a heavy charged particle moving in a metal.^{15,16} Particularly, Fisher and Zwerger¹⁶ have used a model of Ohmic dissipation proposed earlier by Caldeira and Leggett¹⁴ to show that there are two phases at $T = 0$: (i) For weak dissipation, the particle diffuses freely as if the periodic potential were completely absent, and the mobility μ takes its maximum perfect value (free phase). (ii) When the dissipation exceeds a critical value, however, the particle gets localized in a minimum of the potential, and $\mu = 0$ (localized phases). As we adopt the convention in which the dissipation coefficient is fixed at $1/2$ [Eq. (2.6)], the period is given by $a = 1$ at the phase boundary. Later, the above result was rediscovered in the context of single-barrier tunneling in a Luttinger liquid.^{17,30} In the Luttinger liquid model, the above two zero-temperature phases correspond to the two different regimes of the electron-electron interaction which is typically characterized by the Luttinger liquid correlation parameter g . (i) If the interaction is attractive ($g > 1$), electrons can freely tunnel through any arbitrarily strong barrier (free phase). (ii) For a repulsive interaction ($g < 1$), however, even an arbitrarily weak barrier can completely block transport and the conductance vanishes (localized phase).

Another interesting example that is mapped to a 1D QBM model is resonant tunneling of spinless electrons through a quantum dot. In particular, Furusaki and Matveev⁶ have recently studied a system of a quantum dot that is connected to two leads via QPCs. In their model, when an electron tunnels into the dot, each electron in the dot has to pay the Coulomb energy $\sim e^2/C$, where C is the capacitance of the dot. If $e^2/C \gg T$, Coulomb blockade occurs and the tunneling is suppressed unless a nearby gate voltage is tuned in such a way that the Coulomb energy is exactly canceled by the chemical potential of the dot, in which case, resonance occurs. Another assumption of the model is that the dot is large enough that the distance between the point contacts is much greater than the thermal coherence length $L_T = \hbar v_F/k_B T$. In this limit, an electron never travels coherently between the two QPCs. Therefore, if we define Q_1 and Q_2 as the number of electrons in the first and the second lead, respectively, they are independent except through the charge conservation condition

$$n + Q_1 + Q_2 = \text{const.}, \quad (2.11)$$

where n is the number of electrons in the dot. If $e^2/C \gg v_n/\tau_c, T$, charge fluctuation in the dot is suppressed and we may safely integrate out n (or equivalently, $-Q_1 - Q_2$). Then, the resulting effective action has the form of a 1D QBM action in terms of $Q \equiv Q_2 - Q_1$. The current from one lead to the other is $-e\partial_t Q$.

Resonance is achieved when two charge states n and $n + 1$ ($n = \text{integer}$) have the same energy. In that case, electrons no longer pay the penalty when tunneling in and out of the dot. Thus, Coulomb blockade is lifted and current is allowed to pass through the dot down to $T = 0$. If $T > 0$, the conductance is finite even off resonance due to thermal fluctuations. However, it decreases as the gate voltage is tuned away from resonance. In Ref. 6, Furusaki and Matveev have exactly calculated the resonance line shape of the conductance for spinless electrons as a function of gate voltage and temperature. One of the most interesting features of their result is that the resonance line follows a universal one-parameter scaling function

$$G(\delta V_G, T) = \tilde{G} \left(\frac{\delta V_G}{T^{1/2}} \right), \quad (2.12)$$

where δV_G is the deviation of the gate voltage from the on-resonance value. Similar results were obtained for resonant tunneling problems in a Luttinger liquid¹⁸ or between fractional quantum Hall edge states.^{20,31}

Furusaki and Matveev have also argued that the on-resonance behavior of the spinless quantum dot model is governed by the fixed point of the two-channel Kondo problem on the Emery-Kivelson line.³² This limit may be thought of as a generalization of the Toulouse limit in the single-channel Kondo problem¹³ and may be solved exactly.³² In fact, the on-resonance spinless quantum dot model may be shown to be *equivalent* to a Kondo problem on the Emery-Kivelson line. Specifically, it consists of two 1D electron channels and a local magnetic impurity, both of which have spin 1/2. Later, we will rigorously prove the equivalence, but it may be rather straightforwardly visualized via the following one-to-one mappings: (i) the two leads are mapped to the two Kondo channels; (ii) the number of electrons Q_1 and Q_2 are mapped to the z -components of the total spin S_1^z and S_2^z in respective Kondo channels; (iii) the two degenerate charge states of the dot is mapped to the two spin states of the impurity; (iv) the tunneling amplitude t is mapped to the exchange interaction coupling constant J ; (v) the resonance driving gate voltage deviation δV_G is mapped to the local magnetic field \mathcal{H} that applies only to the impurity spin; (vi) the voltage drop between the leads eV is analogous to the difference in the external magnetic field $\mathcal{H}_\epsilon - \mathcal{H}_\infty$ between the channels; (vii) electric conductance G is mapped to the ‘‘spin conductance’’ defined as $\lim_{H_2 \rightarrow H_1} \partial_t (S_2^z - S_1^z) / (\mathcal{H}_\epsilon - \mathcal{H}_\infty)$.

The above Furusaki-Matveev model is quite similar to the spinless Kane-Fisher model of resonant tunneling through a double-barrier in a Luttinger liquid.^{17,18} However, there are several important differences. First of all, the Furusaki-Matveev model assumes no interaction in the lead. Consequently, the quasiparticles have charge $-e$ and the lattice period of the corresponding QBM model is always one. In the Kane-Fisher model, however, Luttinger-liquid correlation g can take any value, and the potential period changes according to g . Another important difference is that in the Furusaki-Matveev model, the single particle energy level spacing ΔE of the dot is much less than T . Therefore, the resonance states in the quantum dot form a continuum. On the contrary, $\Delta E \gg T$ in the Kane-Fisher model and the double-barrier structure has only one resonance state. Consequently, the on-resonance conductance in the Kane-Fisher model is given by the maximum perfect value for a single channel, $G^* = e^2/h$, whereas in the Furusaki-Matveev model, the two QPCs behave like two independent resistors in series, yielding $G^* = e^2/2h$. The difference between the two models becomes even clearer when electrons carry spin. In Kane-Fisher model, the spin excitation in the dot has a gap, which is the level spacing ΔE , but the spin is gapless in the Furusaki-Matveev model since $\Delta E \ll T$.

So far, we have considered only 1D QBM models, where there is only one dynamic variable, namely, Q . If one needs more than one variable for analysis, the above arguments may be extended to higher dimensional QBM models. Such is the case when the spin or transverse degrees of freedom are included into the above two-lead quantum dot model, or when the quantum dot is coupled to multiple leads. As far as low-energy physics is concerned, each 1D electron

channel may be considered equivalent to a lead connected to the dot via a QPC with one transmitting 1D channel. For example, if there are two spin-channels in the two-lead model, it is equivalent to a four-lead model without spin.

We may define the number of electrons Q_i ($i = 1 \cdots N$) for each individual 1D channel, where N is the number of channels. The set of all variables, (Q_1, Q_2, \cdots, Q_N) , can be thought of as the position vector of an N -dimensional quantum Brownian particle. In the weak coupling limit ($v_n/\tau_c \gg T, e^2/C$), all Q 's are strongly quantized at integers. The Brownian particle thus stays most of the time on N -dimensional cubic lattice sites with unit lattice constant ($a = 1$). As in the above analysis, the number of electrons in the dot, $n = \text{const.} - \sum_i Q_i$, may be integrated out at low temperatures ($T \ll e^2/C$). In this process, the dimension of the resulting QBM model is reduced by one and the cubic lattice is projected to the $N - 1$ dimensions.

As the two-lead spinless problem of resonant tunneling is mapped to the two-channel Kondo model, so does the N -channel resonant tunneling problem to the N -channel Kondo model. The mapping will be performed later in two steps. Firstly, in Sec. IV, we will map the N -lead resonant tunneling problem to a QBM model. Then, in Sec. VIII, the N -channel Kondo model will be mapped to the same QBM model. As in the two-lead case, the resonance line shape follows a universal scaling function, of which form may be in principle obtained using the properties of the N -channel Kondo fixed point.

III. RESONANT TUNNELING OF SPINLESS ELECTRONS

In this section, we will formally construct the QBM action for the two-lead spinless quantum dot model discussed in the previous section. Experimentally, one may completely polarize the spin by means of a strong magnetic field. In order to avoid quantum Hall effect, we assume that the magnetic field is parallel to the 2DEG plane. As in Ref. 6, we will assume $\Delta E \ll T \ll e^2/C$, so quantum coherence is thermally destroyed as electrons travel across the dot. This allows us to treat the two QPCs independently. We also suppose that the QPCs transmit only one 1D channel. Following the standard bosonization method,²⁸ we write the Euclidean action as⁶

$$S = S_0 + S_v + S_C, \quad (3.1)$$

where the three terms describe the kinetic energy, backscattering, and the Coulomb energy, respectively. In our units, $\hbar = k_B = 1$.

The kinetic term is explicitly given by

$$S_0 = \sum_a \frac{1}{8\pi v_F} \int d\tau dx [(\partial_\tau \theta_a)^2 + (v_F \partial_x \theta_a)^2], \quad (3.2)$$

where θ_a is the boson field of the a -th lead ($a = 1, 2$) and v_F is the Fermi velocity of the electrons. In accordance with Ref. 6, each QPC has its own coordinate system. In particular, we set $x = 0$ at the center of each QPC and assume $x < 0$ in the dot and $x > 0$ in the leads. Backscattering is assumed to occur right at $x = 0$. Since the density of electrons is given in terms of boson fields by^{17,18,21}

$$\rho_a(x) = \frac{\partial_x \theta_a(x)}{2\pi}, \quad (3.3)$$

the total number of electrons in the a -th lead is given by

$$Q_a = \int_0^\infty dx \rho_a(x) \quad (3.4)$$

$$= -\theta_a(0)/2\pi \quad (3.5)$$

up to a constant.

The backscattering term is given by

$$S_v = -v \sum_{a=1}^2 \int \frac{d\tau}{\tau_c} [e^{i\theta_a(x=0)} + \text{c.c.}], \quad (3.6)$$

where v is a dimensionless backscattering amplitude. This describes an electron backscattered from momentum k_F to $-k_F$ and vice versa ($2k_F$ -backscattering). In real systems, higher harmonics that describe multiple electron scattering ($4k_F$ -backscattering etc.) are also present [See Eq. (2.10)]. As will be shown in Sec. VI, however, they are less

relevant in the renormalization group sense, and it suffices to keep only the single-electron backscattering term in order to discuss low-energy physics. We have also assumed that the two QPCs are identical and thus have the same backscattering amplitude. The effect of asymmetric QPCs will be discussed later at the end of this section. In general, v is a complex number, but without loss of generality it can be always made real by shifting θ_a by a constant.

Finally, the Coulomb energy term can also be written in terms of θ_a . Since the number of electrons in the dot is $n = -(Q_1 + Q_2)$ up to a constant, we may write

$$S_C = \frac{e^2}{2C} \int d\tau \left[\frac{\theta_1(x=0) + \theta_2(x=0)}{2\pi} - n_0 \right]^2, \quad (3.7)$$

where n_0 is proportional to the chemical potential of the dot and is controlled by the gate voltage. Note that n_0 is not integer in general.

Now, we may derive the QBM action by integrating out all degrees of freedom but Q_1 and Q_2 . The resulting effective action is written as

$$\begin{aligned} S_{\text{eff}}[Q_1, Q_2] &= \frac{1}{2} \int d\omega |\omega| [|Q_1(\omega)|^2 + |Q_2(\omega)|^2] \\ &\quad - 2v \int \frac{d\tau}{\tau_c} [\cos 2\pi Q_1(\tau) + \cos 2\pi Q_2(\tau)] \\ &\quad + \frac{e^2}{2C} \int d\tau \{ -[Q_1(\tau) + Q_2(\tau)] - n_0 \}^2. \end{aligned} \quad (3.8)$$

We have replaced the Matsubara frequency sum to an integral, which is a valid approximation at low temperatures. Identifying (Q_1, Q_2) with the position vector of a Brownian particle, the above action describes a two-dimensional (2D) QBM model. The second term above is now mapped to a periodic potential. Clearly, it has a square lattice symmetry with the period $a = 1$. The minima of the periodic potential are explicitly depicted by circles and squares in Q_1 - Q_2 space in Fig. 3. For weak backscattering, one may treat it perturbatively in small v . In the opposite limit (large v), the problem is better described in terms of tunneling between potential minima with a small tunneling amplitude t . This duality will be discussed in more detail in Sec. VI.

If $e^2/C \gg T, v/\tau_c$, then $n = -(Q_1 + Q_2)$ can be safely integrated out. In terms of the new variable $r = (Q_2 - Q_1)/\sqrt{2}$, the final effective action is written as

$$\begin{aligned} S_{\text{eff}}[r] &= \frac{1}{2} \int d\omega |\omega| |r(\omega)|^2 \\ &\quad - 4v \cos \pi n_0 \int \frac{d\tau}{\tau_c} \cos \sqrt{2}\pi r(\tau). \end{aligned} \quad (3.9)$$

Note that the above action has the same form as that of the 1D QBM model in Sec. II, except for an additional n_0 dependent factor in front of the periodic potential and a longer period $a = \sqrt{2}$. According to Fisher and Zwerger,¹⁶ if $a > 1$, the mobility μ vanishes at $T = 0$ for any arbitrarily small amplitude of the periodic potential. In other words, the Brownian particle gets completely trapped in a potential minimum. In the original quantum dot problem, this means that electron tunneling through the dot is completely suppressed at $T = 0$, unless $\cos \pi n_0 = 0$. This is the familiar Coulomb blockade.

If the gate voltage is tuned so that n_0 is exactly a half integer, the periodic potential is identically zero. This is the resonance condition where two charge states $n = n_0 \pm 1/2$ become degenerate. In the QBM description, this corresponds to a degeneracy between two different sets of lattice sites in the Q_1 - Q_2 space. The degenerate lattice sites in Q_1 - Q_2 space forms a ‘‘corrugated 1D lattice’’ as in Fig. 3. Note that the period in the r -direction has now become $a = 1/\sqrt{2}$. The motion in the n -direction gets renormalized down to zero at $T = 0$. Since $a < 1$, the Brownian particle now diffuses freely completely unaffected by the periodic potential at $T = 0$. This implies that Coulomb blockade is lifted and electron current is allowed to flow across the dot.

We want to make a few comments here. Firstly, the resonance fixed point of the two-lead spinless model is the same as the trivial backscattering-free fixed point ($v = 0$). In general, this is not true in higher dimensional QBM models, in which the resonance fixed point is usually inaccessible using a perturbative method. In this case, however, the on-resonance conductance is simply given by the perfect conductance calculated in the absence of backscattering. From the series conductance of two perfect conductors, we get $G = e^2/2h$.

Secondly, the resonance line shape follows a scaling function. If we define δn_0 as the deviation of n_0 from the nearest half integer, one may Taylor expand Eq. (3.9) for small δn_0 to get

$$S_v \approx \pm 4\pi v \delta n_0 \int \frac{d\tau}{\tau_c} \cos \sqrt{2}\pi r + \mathcal{O}(\delta n_0^3). \quad (3.10)$$

As will be shown in Sec. VI, the scaling dimension of δn_0 is given by $1/a^2$. Substituting $a = \sqrt{2}$, we find that the conductance as a function of δn_0 and temperature has the scaling form

$$G(\delta n_0, T) = \tilde{G}\left(\frac{\delta n_0}{T^{1/2}}\right). \quad (3.11)$$

This is consistent with the result in Ref. 6 [See Eq. (2.12)]. Clearly, $\tilde{G}(0) = e^2/2h$ and $\tilde{G}(\infty) = 0$. As will be shown in Sec. VIII, if we map this model to a two-channel Kondo problem, δn_0 is mapped to the magnetic field \mathcal{H} that is locally applied to the magnetic impurity. Since the scaling dimension of \mathcal{H} is $1/2$ [Ref. 33], it is consistent with the above result.

Lastly, we briefly discuss the effect of asymmetric QPCs. If $v_1 \neq v_2$, there is no longer a symmetry between $n = n_0 \pm 1/2$ even if n_0 is a half integer. In fact, the periodic potential never vanishes at any n_0 . Consequently, even the peak value of the conductance resonance vanishes as $T \rightarrow 0$. In this sense, there is no true resonance for asymmetric QPCs. In the renormalization group point of view, the resonance fixed point is unstable with respect to the asymmetry. However, even if the QPCs are not perfectly symmetric, if $|v_1 - v_2|/\tau_c \ll T$, the flow will not have crossed over to the asymmetric fixed point and the system is still governed by the resonance fixed point.

IV. MULTI-LEAD RESONANT TUNNELING MODELS

In this section, we will generalize the above analysis to a general N -lead case and show that it is mapped to a $(N - 1)$ -dimensional QBM model.

The first example is the three-lead model shown in Fig. 4(a). As in the two-lead case, we define the total number of electrons in each lead Q_a ($a = 1, 2, 3$) and treat them as vector components of the three-dimensional (3D) position of a Brownian particle. Charge conservation law again asserts that $n = -(Q_1 + Q_2 + Q_3)$ up to a constant. Assuming the three QPCs are symmetric, the total QBM action looks similar to the one in Eq. (3.8) except for the third variable Q_3 . Again, in the strong backscattering limit ($v/\tau_c \gg T, e^2/C$), Q_a are strongly quantized in order to minimize the potential energy. Since the potential has a cubic lattice symmetry with lattice constant $a = 1$, the minima also form a cubic lattice [Fig. 4(b)]. The Brownian particle propagates by hopping between these lattice sites. At low temperatures ($T \ll e^2/C$), n is integrated out and takes an integer value that minimizes the Coulomb energy. In terms of Q_a , this condition is

$$Q_1 + Q_2 + Q_3 = -n = \text{integer const.}, \quad (4.1)$$

which defines a plane perpendicular to the (111) direction. Fig. 4(b) shows two examples of such planes viewed from the (111) direction. On any plane, the subset of lattice sites clearly form a triangular lattice with lattice constant $a = \sqrt{2}$. Off resonance, n is allowed to take only one value, and the Brownian particle stays on only one plane. However, when n_0 is a half integer (on resonance), the system is allowed to hop between two planes corresponding to $n = n_0 \pm 1/2$. As sketched in Fig. 4(b), they form a ‘‘corrugated honeycomb lattice’’ composed of two parallel triangular sublattice planes.

We may generalize the above analysis to an N -lead system. In the strong backscattering limit, the coordinates (Q_1, Q_2, \dots, Q_N) form an N -dimensional generalization of a cubic lattice with $a = 1$. When $e^2/C \gg T$, depending on whether off or on resonance, the Brownian particle is constrained within one or two $(N - 1)$ -dimensional lattices on ‘‘hyper-planes’’ perpendicular to the $(11 \dots 1)$ direction. It is straightforward to show that the lattice on each hyper-plane is an $(N - 1)$ -dimensional *symmorphic*³⁴ close-packed lattice with $a = \sqrt{2}$. We will call it an ‘‘ $(N - 1)$ -dimensional triangular lattice’’. On resonance ($n_0 = \text{half integer}$), two adjacent hyper-planes are degenerate and the two $(N - 1)$ -dimensional triangular sublattices are combined to form an ‘‘ $(N - 1)$ -dimensional honeycomb lattice’’. For example, if $N = 4$, a 3D triangular lattice (off resonance) is, in fact, a face-centered cubic (FCC) lattice,³⁵ and a 3D honeycomb lattice (on resonance) is a diamond lattice. Note that a diamond lattice is made of two FCC sublattices.

Now we present a formal derivation of the QBM action from the N -lead resonant tunneling model. Generalizing Eq. (3.8), we may write

$$S_{\text{eff}}[\{Q_a\}] = \sum_{a=1}^N \left\{ \frac{1}{2} \int d\omega |\omega| |Q_a(\omega)|^2 - v \int \frac{d\tau}{\tau_c} \cos 2\pi Q_a(\tau) \right\} + \frac{e^2}{2C} \int d\tau \left\{ - \left[\sum_{a=1}^N Q_a(\tau) \right] - n_0 \right\}^2. \quad (4.2)$$

For convenience, we perform change of variables

$$\begin{bmatrix} r_i \\ \nu \end{bmatrix} = \mathbf{O} \begin{bmatrix} Q_a \end{bmatrix}, \quad (i = 1 \cdots N-1), \quad (4.3)$$

where \mathbf{O} is an orthogonal matrix which is defined in such a way that the last component of the left-hand side of the above equation is given by

$$\nu \equiv \frac{1}{\sqrt{N}} \sum_a Q_a = -\frac{n}{\sqrt{N}}. \quad (4.4)$$

After ν is integrated out, the effective action becomes

$$\begin{aligned} S_{\text{eff}}[\{r_i\}] &= \frac{1}{2} \int d\omega |\omega| \sum_{i=1}^{N-1} |r_i|^2 \\ &\quad - v \sum_{a=1}^N \int \frac{d\tau}{\tau_c} \cos 2\pi \left[\sum_{i=1}^{N-1} \mathbf{O}_{ai}^{-1} r_i(\tau) - \frac{n_0}{N} \right], \end{aligned} \quad (4.5)$$

which is an $(N-1)$ -dimensional QBM action. The minima of the periodic potential in $\{r_i\}$ space form an $(N-1)$ -dimensional triangular lattice unless n_0 is a half integer, in which case they form an $(N-1)$ -dimensional honeycomb lattice. The zero-temperature phase diagrams of these lattice models will be derived in Sec. VII.

V. RESONANT TUNNELING IN A LUTTINGER LIQUID

A similar analysis as above may be performed for resonant tunneling of a 1D Luttinger liquid in a double-barrier structure. Let us first discuss the spinless case. Following Ref. 18, we suppose that there are δ -function barriers at $x=0$ and $x=d$. The Euclidean action in the bosonized form is given by

$$S = \frac{1}{8\pi g v_s} \int d\tau dx [(\partial_\tau \theta)^2 + (v_s \partial_x \theta)^2] + eV_G \int d\tau [\theta(d) - \theta(0)] + v \int \frac{d\tau}{\tau_c} \{\cos[\theta(0)] + \cos[\theta(d)]\}, \quad (5.1)$$

where v_s is the sound velocity, g is the Luttinger-liquid correlation, and V_G is the gate voltage near the isolated region $0 < x < d$. If the electron-electron interaction is repulsive (attractive), the Luttinger-liquid correlation parameter satisfies $g < 1$ ($g > 1$). After $\theta(x)$ is integrated out except at $x=0$ and d , we get the effective action

$$S_{\text{eff}}[Q, n] = \frac{1}{g} \int d\omega |\omega| \left[\frac{|Q(\omega)|^2}{1 + e^{-|\omega|d/v_s}} + \frac{1}{4} \frac{|n(\omega)|^2}{1 - e^{-|\omega|d/v_s}} \right] + eV_G \int d\tau n(\tau) + v \int \frac{d\tau}{\tau_c} \cos 2\pi Q(\tau) \cos \pi n(\tau), \quad (5.2)$$

where

$$Q = \frac{\theta(0) + \theta(d)}{4\pi}, \quad (5.3)$$

$$n = \frac{\theta(d) - \theta(0)}{2\pi}. \quad (5.4)$$

Q is the number of electrons that has transferred from one side of the double-barrier to the other and n is the number of electrons between the barriers.

Since there is an energy gap $\Delta E = v_s/gd$ for $n(\omega)$ as $\omega \rightarrow 0$, we may safely integrate it out for $|\omega| \ll \Delta E$. The low frequency part of the action is then written as

$$S_{\text{eff}}[r] = \frac{1}{2} \int d\omega |\omega| |r(\omega)|^2 + v \cos \pi n_0 \int \frac{d\tau}{\tau_c} \cos 2\pi \sqrt{g} r(\tau), \quad (5.5)$$

where $r \equiv Q/\sqrt{g}$ and $n_0 = eV_G gd/v_s$.

The above action closely resembles that of the two-lead quantum dot model in Eq. (3.9). However, there are a few important differences. First of all, the potential period is $1/\sqrt{g}$ in the Luttinger liquid, which varies with the electron-electron interaction, whereas it is fixed at $\sqrt{2}$ in the quantum dot model. Another important difference is

that the level spacing ΔE is finite in the Luttinger liquid model. Thus, at low temperatures ($T \ll \Delta E$), the thermal coherence length $L_T = \hbar v_s / k_B T$ is much greater than the barrier separation d . In other words, when electrons tunnel through the double-barrier, they fully retain their phase information. Therefore, a single boson field $\theta(x)$ has been used for both barriers, whereas in the quantum dot model, each QPC was described by an independent field $\theta_a(x)$. Consequently, the two models are not the same even in the non-interacting limit of the Luttinger liquid ($g = 1$). In that limit, the period is one for the Luttinger liquid model and the on-resonance conductance is given by $G^* = e^2/h$, which differs from that of the two-lead quantum dot model by a factor of 2. The resonance line shape also has a different scaling form,

$$G(\delta n_0, T) = \tilde{G} \left(\frac{\delta n_0}{T^{1-g}} \right). \quad (5.6)$$

Interestingly, the Luttinger liquid model yields the same on-resonance conductance and resonance scaling function as the two-lead quantum dot model, if $g = 1/2$.

A similar analysis is possible when there is spin degree of freedom. Now we need two boson fields θ_\uparrow and θ_\downarrow for up and down spin states. It is convenient to define charge and spin fields

$$\theta_\rho = \theta_\uparrow + \theta_\downarrow, \quad (5.7)$$

$$\theta_\sigma = \theta_\uparrow - \theta_\downarrow. \quad (5.8)$$

The effective action is given by

$$S_{\text{eff}}[\{Q_\alpha\}, \{n_\alpha\}] = \sum_{\alpha=\rho,\sigma} \frac{1}{g_\alpha} \int d\omega |\omega| \left[\frac{|Q_\alpha(\omega)|^2}{1 + e^{-|\omega|d/v_s}} + \frac{1}{4} \frac{|n_\alpha(\omega)|^2}{1 - e^{-|\omega|d/v_s}} \right] + \int \frac{d\tau}{\tau_c} [eV_G n_\rho(\tau) + \mathcal{H} n_\sigma(\tau)] + S_v, \quad (5.9)$$

where \mathcal{H} is the magnetic field applied *only between the barriers* and S_v contains all allowed backscattering processes. g_ρ and g_σ are Luttinger-liquid correlations for the charge and spin sectors, respectively. If there is SU(2) spin symmetry, $g_\sigma = 2$. In the non-interacting limit, $g_\rho = g_\sigma = 2$. Physically, Q_σ means the total spin that has transferred across the barriers and n_σ means the total spin between the barriers (both in units of $\hbar/2$). Q_ρ and n_ρ have similar meanings except that they are defined for number of electrons. Note that both n_ρ and n_σ have an energy gap, whereas in the quantum dot model, only n_ρ has a gap.

After both n_ρ and n_σ are integrated out, the above effective action describes a 2D QBM in terms of Q_ρ and Q_σ . Particularly in the vicinity of $g_\rho = 1$ and $g_\sigma = 3$, Kane and Fisher have found a fixed point similar to the intermediate fixed point of the QBM model on a 2D honeycomb lattice.¹⁸ There, the most relevant backscattering terms are

$$S_v = \int \frac{d\tau}{\tau_c} [v_e \cos \pi Q_\rho \cos \pi Q_\sigma + v_1 \cos 2\pi Q_\rho + v_2 \sin 2\pi Q_\rho], \quad (5.10)$$

where all v 's are real-valued. Physically, the first term describes backscattering of a single electron and the other two backscattering of a spin-singlet pair. Defining rescaled variables

$$r_\rho = Q_\rho / \sqrt{g_\rho}, \quad r_\sigma = Q_\sigma / \sqrt{g_\sigma}, \quad (5.11)$$

the low-frequency effective action is written as

$$S_{\text{eff}}[r_\rho, r_\sigma] = \frac{1}{2} \int d\omega |\omega| [|r_\rho(\omega)|^2 + |r_\sigma(\omega)|^2] + \int \frac{d\tau}{\tau_c} (v_e \cos \pi \sqrt{g_\rho} r_\rho \cos \pi \sqrt{g_\sigma} r_\sigma + v_1 \cos 2\pi \sqrt{g_\rho} r_\rho + v_2 \sin 2\pi \sqrt{g_\rho} r_\rho). \quad (5.12)$$

If $g_\sigma/g_\rho = 3$, $v_e = 2v_1$, and $v_2 = 0$, the above action has a honeycomb lattice symmetry in the r_ρ - r_σ plane. For $g_\sigma/g_\rho \neq 3$, the lattice is stretched or compressed. The fixed point of this ‘‘distorted honeycomb lattice’’ will be discussed in Sec. VII E.

VI. GENERAL FORMALISM OF THE QBM MODEL

In this section, we will present a general formalism of the QBM model with a periodic potential and its renormalization group analysis. Specific lattice models will be discussed in the following section. In any arbitrary dimensions a generic QBM action is written as

$$S = S_0 + S_v, \quad (6.1)$$

where

$$S_0 = \frac{1}{2} \int d\omega |\omega| e^{|\omega|\tau_c} |\mathbf{r}(\omega)|^2, \quad (6.2)$$

$$S_v = - \int \frac{d\tau}{\tau_c} \sum_{\mathbf{G}} v_{\mathbf{G}} e^{i2\pi\mathbf{G}\cdot\mathbf{r}(\tau)}. \quad (6.3)$$

The above two terms represent the dissipative kinetic energy and the periodic potential, respectively. $\mathbf{r}(\tau)$ is the trajectory of the Brownian particle as a function of imaginary time τ and $v_{\mathbf{G}}$ is a dimensionless amplitude of the potential at a reciprocal lattice vector \mathbf{G} . In Eq. (6.2), high frequency fluctuations are exponentially suppressed by τ_c . The potential minima form a lattice $\{\mathbf{R}\}$, where

$$\mathbf{G} \cdot \mathbf{R} = \text{integer}, \quad (6.4)$$

for any \mathbf{G} and \mathbf{R} . The dissipation is proportional to the coefficient in the righthand side of Eq. (6.2), but it may be absorbed into \mathbf{G} by rescaling \mathbf{r} and \mathbf{G} appropriately. As dissipation gets stronger, $|\mathbf{R}|$ increases and $|\mathbf{G}|$ decreases.

Now let us discuss the linear response of the Brown particle to a uniform external force \mathbf{F} . Firstly, we add the following term to the total action:

$$S_{\mathbf{F}} = - \int d\tau \mathbf{F} \cdot \mathbf{r}(\tau). \quad (6.5)$$

Then the mobility μ_{ij} is defined as the ratio of the average velocity of the Brownian particle to the external force, in the linear response regime. Following standard linear response theory, it is written as

$$\mu_{ij} \equiv \lim_{\mathbf{F} \rightarrow 0} \frac{\partial}{\partial F_j} \langle \partial_t r_i \rangle, \quad (6.6)$$

$$= \lim_{\omega \rightarrow 0} \frac{1}{|\omega|} \int d\omega' \omega \omega' \langle r_i(\omega) r_j(-\omega') \rangle, \quad (6.7)$$

$$= \mu \delta_{ij}. \quad (6.8)$$

In the last line we assumed that the mobility is isotropic. Note that it is normalized in such a way that $\mu = 1$ (“perfect mobility”), if $v_{\mathbf{G}} = 0$.

In the weak potential limit ($v_{\mathbf{G}} \ll 1$), it is natural to construct a perturbation theory in small $v_{\mathbf{G}}$. In order to study low-temperature properties, we perform a renormalization group analysis analogous to the ones in Ref. 18. The general scheme of the renormalization group analysis is described in Appendix A. Up to the leading order in $v_{\mathbf{G}}$, the renormalization group flow equation is given by

$$\frac{dv_{\mathbf{G}}}{d\ell} = (1 - |\mathbf{G}|^2) v_{\mathbf{G}}. \quad (6.9)$$

Clearly, all $v_{\mathbf{G}}$ are irrelevant if the shortest reciprocal lattice vector satisfies $|\mathbf{G}_0|^2 < 1$.

On the other hand, if $v_{\mathbf{G}} \gg 1$, the Brownian particle is more likely to be localized at a minimum \mathbf{R} of the potential. In that case, transport is dominated by tunneling between potential minima, and the partition function may be expanded in powers of the fugacity of tunneling events. In order to describe tunneling, it is more convenient to write the action in terms of $\mathbf{k}(\tau)$, which is the trajectory of the particle in the momentum space. The new action, which is dual to Eq. (6.1), is given by

$$S = S_0 + S_t, \quad (6.10)$$

where

$$S_0 = \frac{1}{2} \int d\omega |\omega| e^{|\omega|\tau_c} |\mathbf{k}(\omega)|^2, \quad (6.11)$$

$$S_t = - \int \frac{d\tau}{\tau_c} \sum_{\mathbf{R}} t_{\mathbf{R}} e^{i2\pi\mathbf{R}\cdot\mathbf{k}(\tau)}. \quad (6.12)$$

The two terms represent the kinetic energy and the tunneling, respectively. $t_{\mathbf{R}}$ is the tunneling amplitude between two lattice sites connected by a displacement vector \mathbf{R} . The mobility is written as

$$\mu_{ij} = \delta_{ij} - \lim_{\omega \rightarrow 0} \frac{1}{|\omega|} \int d\omega' \omega \omega' \langle k_i(\omega) k_j(-\omega') \rangle. \quad (6.13)$$

Since the dual action has exactly same form as the original action, it is straightforward to obtain the renormalization group flow equation

$$\frac{dt_{\mathbf{R}}}{d\ell} = (1 - |\mathbf{R}|^2)t_{\mathbf{R}}. \quad (6.14)$$

From the above flow equations one can easily find two trivial fixed points: the localized ($t_{\mathbf{R}} = 0$) and the free ($v_{\mathbf{G}} = 0$) fixed points. The mobility at the fixed points is simply given by $\mu = 0$ and $\mu = 1$, respectively. Other fixed points will be obtained and analyzed in the next section.

VII. LATTICE MODELS AND PHASE DIAGRAMS

In this section, we study the properties of the QBM model with various lattice symmetries. Using a renormalization group analysis, we will derive the phase diagram of each lattice.

A lattice is either symmorphic or non-symmorphic depending on the crystallographic space group of the coordinate transformations that leave the system invariant. If the space group is a semi-direct product of a pure translation group and a pure rotation group, it is called symmorphic. Otherwise, it is non-symmorphic.³⁴ For example, all Bravais lattices are symmorphic, and the honeycomb, Kagomé, and diamond lattices are non-symmorphic. One of the major results of this paper is the proof that there is a stable intermediate fixed point only for non-symmorphic lattices. The first two subsections below deal with symmorphic lattices and the following three with non-symmorphic lattices.

A. One-dimensional lattice

The simplest example of a symmorphic lattice is a 1D lattice. According to Eq. (6.4) the lattice sites in the direct and the reciprocal lattice are given by

$$R = mR_0, \quad (7.1)$$

$$G = n/R_0, \quad (7.2)$$

where R_0 is the lattice constant, and m and n are integers. It follows from Eqs. (6.9) and (6.14) that

$$\frac{dv_G}{d\ell} = (1 - n^2/R_0^2)v_G, \quad (n \neq 0), \quad (7.3)$$

$$\frac{dt_R}{d\ell} = (1 - m^2R_0^2)t_R, \quad (m \neq 0). \quad (7.4)$$

From the above equations, it is obvious that if $R_0 < 1$, all v_G are irrelevant, whereas t_R is relevant at least for $m = \pm 1$. Now suppose that the bare value of $t_R (m = \pm 1)$ is perturbatively small. If the system is scaled down to lower energies under successive renormalization group transformations, t_R will keep growing until eventually it departs from the perturbative regime. Presumably, the system will continuously flow towards the opposite limit where v_G is small. Under further renormalization group transformations, v_G will decrease until it vanish at $T = 0$. In more formal words, the localized fixed point ($t_R = 0$) is unstable and the free fixed point ($v_G = 0$) is stable. At $T = 0$, the Brownian particle diffuses completely unaffected by the periodic potential.

In contrast, if $R_0 > 1$, all t_R are irrelevant whereas v_G is relevant at least for $n = \pm 1$. Now, exactly the opposite happens under renormalization group transformations. In short, the free fixed point ($v_G = 0$) is unstable and the localized fixed point ($t_R = 0$) is stable. The zero-temperature phase is now localized and the particle gets completely trapped in a minimum of the potential at $T = 0$.

The physical interpretation of these is as follows. For $R_0 < 1$, the lattice sites are close enough for a given dissipation strength — or the dissipation is weak enough for a given lattice constant — that the Brownian particle tunnels easily at low temperatures. If $R_0 > 1$, however, lattice sites are far apart or the dissipation is too strong that the particle

can hardly tunnel. In fact, the above result is a reproduction of the result of a 1D QBM model in Ref. 16 and of a single-barrier spinless Luttinger liquid model in Ref. 18. In the latter model, the Luttinger-liquid correlation parameter g is related to the lattice constant by

$$g = 1/R_0^2. \quad (7.5)$$

The above free and localized phases are equivalent to the fully coherently transmitting phase of the Luttinger liquid model for attractive interactions ($g > 1$, $R_0 < 1$) and the insulating phase for repulsive interactions ($g < 1$, $R_0 > 1$), respectively.

The above result may be summarized in terms of the zero-temperature universal mobility

$$\mu^* = \begin{cases} 0 & \text{if } G_0 < 1, \\ 1 & \text{if } G_0 > 1. \end{cases} \quad (7.6)$$

Note that the zero-temperature phase is completely independent of v or t . The phase transition is solely controlled by R_0 .

In order to determine the zero-temperature phase, it is sufficient to consider only the shortest lattice vectors \mathbf{R}_0 and \mathbf{G}_0 , because they are the most relevant operators in the respective perturbative regime. Throughout this paper, we will ignore all the other less relevant lattice vectors. However, one can easily include less relevant operators when it is necessary.

Without many modifications, the above analysis may be applied to square lattices, cubic lattices, and their higher-dimensional generalization. In the vicinity of the phase boundary $|\mathbf{G}_0|^2 = 1$, each vector component of \mathbf{r} or \mathbf{k} gets completely decoupled from the others at $T = 0$, since all the coupling terms such as $e^{i2\pi(r_1+r_2)}$ are irrelevant. Therefore, the square lattice and its higher dimensional generalizations can be treated as a set of independent 1D lattices.

B. Triangular lattice and its D -dimensional generalization

We argued in Sec. IV that the off-resonance multi-lead quantum dot model is mapped to the QBM model on a multi-dimensional triangular lattice. In this subsection, we will first analyze the 2D triangular lattice model, and then generalize it to higher dimensions.

The reciprocal lattice of a triangular lattice is also a triangular lattice. We will assume that there is a six-fold symmetry and the potential amplitudes are positive for the six shortest reciprocal lattice vectors \mathbf{G}_0 , i.e.,

$$v_{\mathbf{G}_0} = v = \text{const.} > 0. \quad (7.7)$$

From the six-fold symmetry, it also follows that

$$t_{\mathbf{R}_0} = t = \text{const.} \quad (7.8)$$

It is straightforward to see that

$$|\mathbf{G}_0|^2 |\mathbf{R}_0|^2 = \frac{4}{3}. \quad (7.9)$$

A simple renormalization group analysis as in the previous subsection shows that if $|\mathbf{G}_0|^2 > 4/3$ and $|\mathbf{R}_0|^2 < 1$, the free fixed point is stable and the localized fixed point is unstable. If $|\mathbf{G}_0|^2 < 1$ and $|\mathbf{R}_0|^2 > 4/3$, the localized fixed point is stable and the free fixed point is unstable. However, if $1 < |\mathbf{G}_0|^2, |\mathbf{R}_0|^2 < 4/3$, both fixed points are stable and there is at least one unstable fixed point between them. Physically, this means that there are at least two distinct phases at $T = 0$: free and localized. Although it is very unlikely that there are more fixed points, we currently do not have an evidence to completely rule out the possibility. Assuming there are only two stable fixed points, the zero-temperature phase depends on whether the bare value of v is above or below the unstable intermediate fixed point. As v moves from one side of the unstable fixed point to the other, a first order phase transition occurs at $T = 0$ and the mobility jumps between zero and one.

For small v , the intermediate fixed point may be perturbatively accessed near $|\mathbf{G}_0|^2 = 1$. More specifically, we introduce a small parameter $\epsilon > 0$ and perform a perturbative renormalization group analysis at $|\mathbf{G}_0|^2 = 1 + \epsilon$. Since details of the analysis will be given in Appendix A, here we will just state the result. The renormalization group flow equation is given by

$$\frac{dv}{d\ell} = -\epsilon v + 2v^2. \quad (7.10)$$

Solving $dv/d\ell = 0$, we get the intermediate fixed point

$$v^* = \frac{\epsilon}{2}. \quad (7.11)$$

The scaling dimension of the most relevant operator at the fixed point is

$$\Delta = 1 - \epsilon. \quad (7.12)$$

Using Eq. (6.7), we may also compute the universal fixed point mobility

$$\mu^* = 1 - \frac{3\pi^2}{2}\epsilon^2. \quad (7.13)$$

A similar perturbative analysis was used in Ref. 18.

The analysis for small t near $|\mathbf{R}_0|^2 = 1$ is very similar. In fact, since both the direct and reciprocal lattices are triangular, one may directly use the duality. Namely, the small v limit is mapped exactly to the small t limit if the following substitutions are made:

$$\mathbf{r} \rightarrow \mathbf{k}, \quad (7.14)$$

$$\mathbf{G} \rightarrow \mathbf{R}, \quad (7.15)$$

$$v \rightarrow t. \quad (7.16)$$

The mobility μ is then mapped to $1 - \mu$. At $|\mathbf{R}_0|^2 = 1 + \epsilon$, the results can be directly read off from Eq. (7.10) through Eq. (7.13). Explicitly, they are

$$\frac{dt}{d\ell} = -\epsilon t + 2t^2, \quad (7.17)$$

$$t^* = \frac{\epsilon}{2}, \quad (7.18)$$

$$\Delta = 1 - \epsilon, \quad (7.19)$$

$$\mu^* = \frac{3\pi^2}{2}\epsilon^2. \quad (7.20)$$

Note that there is a self-dual point at $|\mathbf{G}_0|^2 = |\mathbf{R}_0|^2 = \sqrt{3}/2$ where the dual models become identical. The mobility at the self-dual point is obviously given by

$$\mu_{\text{sd}}^* = 1 - \mu_{\text{sd}}^* = 1/2. \quad (7.21)$$

It is very hard to calculate the intermediate fixed point away from the above two perturbative limits and the self-dual point. However, assuming that the fixed-point lines on both limits smoothly join together at the self-dual point, one may complete the phase diagram as shown in Fig. 5(a). The top and bottom lines of the figure depicts the free ($v = 0$) and the localized ($t = 0$) fixed points, respectively. The intermediate fixed-point line is also drawn along with the renormalization group flows. The above results may be summarized in terms of the fixed-point mobility

$$\mu^* = \begin{cases} 0 & \text{if } |\mathbf{G}_0|^2 < 1, \\ 0 \text{ or } 1 & \text{if } 1 < |\mathbf{G}_0|^2 < 4/3, \\ 1 & \text{if } |\mathbf{G}_0|^2 > 4/3. \end{cases} \quad (7.22)$$

Unlike in the 1D lattice problem, v and t control a first order phase transition, if $1 < |\mathbf{G}_0|^2 < 4/3$.

Now, let us generalize the above analysis to the D -dimensional triangular lattice. As discussed in Sec. IV, a D -dimensional triangular lattice is defined as a subset of the lattice sites of a $(D + 1)$ -dimensional cubic lattice, that are constrained to a hyper-plane perpendicular to the $(11 \cdots 1)$ direction. Its lattice sites are equivalent to the minima of the off-resonance backscattering action of the $(D + 1)$ -lead quantum dot model [Eq. (4.5) with $n_0 \neq \text{half integer}$], except for that $|\mathbf{R}_0|$ is no more fixed at $\sqrt{2}$. Specifically, it is a conventional triangular lattice for $D = 2$ and an FCC for $D = 3$. It is hard to visualize an object in dimensions greater than three, but it is helpful to illustrate the D -dimensional triangular lattice using an induction argument. For example, we can construct an FCC from a

2D triangular lattice in the following way: A triangular lattice is made of periodically placed equilateral triangles. Likewise, an FCC is made of equilateral tetrahedrons. A tetrahedron in an FCC consists of a triangle at the bottom and the fourth vertex placed above the triangle plane. Due to periodicity, this last vertex also belongs to a triangle in another plane parallel to the first. In other words, an FCC is obtained by stacking up planes of triangular lattices. However, it has to be done in a certain way that the resulting lattice is a *symmorphic* close-packed structure.³⁵ In general, a D -dimensional triangular lattice is obtained by stacking up $(D - 1)$ -dimensional triangular lattice hyperplanes.

Now we may perform a similar renormalization group analysis as above. If $D \geq 3$, however, the reciprocal lattice $\{\mathbf{G}\}$ is no longer the same as the direct lattice $\{\mathbf{R}\}$ and we cannot use duality. (For example, the reciprocal of an FCC is a BCC.) From a geometrical consideration, we find

$$|\mathbf{G}_0|^2 |\mathbf{R}_0|^2 = \frac{2D}{D+1}. \quad (7.23)$$

If $1 < |\mathbf{G}_0|^2 < 2D/(D+1)$, there is an unstable fixed point that separates the localized and the free phases. The phase diagram is schematically drawn in Fig. 5(b). We may also perform an ϵ -expansion analysis analogous to the above. The results are listed in Table I at $|\mathbf{G}_0|^2 = 1 + \epsilon$ in the small v limit. In the opposite limit of small t , the results are given in Table II at $|\mathbf{R}_0|^2 = 1 + \epsilon$.

Before we move on to non-symmorphic lattices, we would like to discuss briefly that the symmetry of the lattice is crucial on determining the phase diagram. For any arbitrary Bravais lattice, $|\mathbf{G}_0| |\mathbf{R}_0| > 1$, and obviously, at least one of $|\mathbf{G}_0|$ and $|\mathbf{R}_0|$ is greater than one. Therefore, it follows from Eqs. (6.9) and (6.14) that at least one trivial fixed point is stable for any arbitrary lattice constant. On the contrary, for a non-Bravais lattice, $|\mathbf{G}_0|$ and $|\mathbf{R}_0|$ may be less than one at the same time, in which case both trivial fixed points are unstable. Then, there must be a stable intermediate fixed point between them. It is indeed the case for the non-symmorphic lattices such as the honeycomb and the diamond lattice. A common feature of all non-symmorphic lattices is that they are made of Bravais sublattices and there is a geometrical symmetry between the sublattices. Since the asymmetry between sublattices is always relevant, even if the symmetry is slightly broken, one sublattice will dominate the others after repetitive renormalization group transformations. Then, the problem reduces to that of the dominating sublattice, which is a symmorphic lattice. Therefore, it is the extra symmetry between sublattices that prevents this ‘‘renormalization of basis’’, and non-symmorphicity is a necessary condition for the existence of a stable intermediate fixed point.

C. Honeycomb lattice and its D -dimensional generalization

In this and the following two subsections, we will study non-symmorphic lattice models. The first example that will be discussed in this subsection is the D -dimensional honeycomb lattice. Following the framework of the the previous subsection, we will first consider the conventional 2D honeycomb lattice, and then generalize it to higher dimensions.

A honeycomb lattice is made of two triangular sublattices. As depicted in Fig. 6, the six shortest lattice vectors $\mathbf{R}_0 \in \{\pm \mathbf{R}_a\}$ ($a = 1, 2, 3$) always connect one sublattice to the other. Note that $\mathbf{R}_0 \in \{\mathbf{R}_a\}$ on A sublattice and $\mathbf{R}_0 \in \{-\mathbf{R}_a\}$ on B sublattice. The reciprocal lattice $\{\mathbf{G}\}$ is a triangular lattice and the six shortest reciprocal lattice vectors are drawn in Fig. 7(a) as $\mathbf{G}_0 \in \{\pm \mathbf{G}_a\}$ ($a = 1, 2, 3$). It is straightforward to see that

$$|\mathbf{G}_0|^2 |\mathbf{R}_0|^2 = \frac{4}{9}. \quad (7.24)$$

From Eqs. (6.9) and (6.14), it follows that for $4/9 < |\mathbf{G}_0|^2 < 1$, both the free and localized fixed points are *unstable*. It implies that there must be at least one stable fixed point between the two. Again, we will assume that there is only one stable fixed point. At the new stable fixed point, the mobility takes a universal value between zero and one ($0 < \mu^* < 1$).

Now let us perform an ϵ -expansion analysis similar to the one in the previous subsection. Computing the structure factor, the potential amplitudes are given by

$$v_{\mathbf{G}_0} = v(1 + e^{i2\pi \mathbf{G}_0 \cdot \mathbf{R}_0}) = v e^{\pm i\pi/3}, \quad (7.25)$$

where we have chosen the origin of the 2D space to lie on an A-sublattice site. The sign in the exponent is (+) if $\mathbf{G}_0 \in \{\mathbf{G}_a\}$ and it is (-) if $\mathbf{G}_0 \in \{-\mathbf{G}_a\}$. Using the above equation, the periodic potential part of the action may be written as

$$S_v = - \int \frac{d\tau}{\tau_c} \sum_{\mathbf{G}_0} v_{\mathbf{G}_0} e^{i2\pi\mathbf{G}_0 \cdot \mathbf{r}} \quad (7.26)$$

$$= -2v \int \frac{d\tau}{\tau_c} \sum_{a=1}^3 \cos\left(2\pi\mathbf{G}_a \cdot \mathbf{r} - \frac{\pi}{3}\right). \quad (7.27)$$

Since a trip around a triangular plaquette in the reciprocal lattice space gives rise to a phase $\pm\pi$ [Fig. 7(b)], this problem may be also viewed as a tight-binding representation of a triangular lattice in which a flux π is threaded in each plaquette with alternating sign.

The ϵ -expansion analysis in the small v limit near $|\mathbf{G}_0|^2 = 1$ is essentially the same as that of a triangular lattice except for the extra factor $e^{\pm i\pi/3}$ in Eq. (7.25). The results are summarized in Table I. In the opposite limit of small t near $|\mathbf{R}_0|^2 = 1$, however, the situation is more complicated due to the two sublattices. When many tunneling events occur sequentially, \mathbf{R}_0 must be alternately chosen from $\{\mathbf{R}_a\}$ and $\{-\mathbf{R}_a\}$. Technically, this is automatically taken care of by using the Pauli matrices $\sigma^\pm = \sigma^x \pm i\sigma^y$. The tunneling part of the action may be written as

$$S_t = -t \int \frac{d\tau}{\tau_c} \sum_a \left(\frac{\sigma^+}{2} e^{i2\pi\mathbf{R}_a \cdot \mathbf{k}} + \frac{\sigma^-}{2} e^{-i2\pi\mathbf{R}_a \cdot \mathbf{k}} \right). \quad (7.28)$$

The alternation between $\{\mathbf{R}_a\}$ and $\{-\mathbf{R}_a\}$ is ensured by the identity $(\sigma^\pm)^2 = 0$. Details of the ϵ -expansion calculation is given in Appendix A. The results may be summarized as follows:

$$\frac{dt}{d\ell} = \epsilon t - 3t^3, \quad (7.29)$$

$$t^* = \sqrt{\frac{\epsilon}{3}}, \quad (7.30)$$

$$\Delta = 1 + 2\epsilon, \quad (7.31)$$

$$\mu^* = \pi^2 \epsilon. \quad (7.32)$$

Fig. 8(a) shows the phase diagram of the honeycomb lattice. Since the stable intermediate fixed-point line smoothly connects the localized and the free phases, there is no first order phase transition as in symmorphic lattices. The fixed point mobility μ^* is also a continuous function of $|\mathbf{G}_0|^2$. In general, the calculation of μ^* is not easy for an arbitrary $|\mathbf{G}_0|^2$, but as will be shown in the Sec. VIII, an exact solution may be obtained for the special case where $|\mathbf{G}_0|^2 = 2/3$, using the mapping of the honeycomb lattice model to the Toulouse limit of the three-channel Kondo model.

Now let us generalize the above analysis to $D \geq 3$. First of all, we define a D -dimensional honeycomb lattice as a subset of the lattice sites of a $(D+1)$ -dimensional cubic lattice, that lie on two adjoining hyper-planes perpendicular to the $(11 \cdots 1)$ direction. Its lattice sites coincide with the minima of the on-resonance backscattering action of the $(D+1)$ -lead quantum dot model [Eq. (4.5) with $n_0 = \text{half integer}$], except for that $|\mathbf{R}_0|$ is no longer fixed. For example, a “3D honeycomb lattice” is a diamond lattice. As a honeycomb lattice consists of two triangular sublattices and a diamond lattice consists of two interpenetrating FCC sublattices, a generic D -dimensional honeycomb lattice consists of two interpenetrating D -dimensional triangular sublattices. Among the two basis sites of a D -dimensional honeycomb lattice, if one is placed at a vertex of a D -dimensional equilateral $(D+1)$ -hedron, the other is at the center.

Generalizing Eqs. (7.24) through (7.28), we get

$$|\mathbf{R}_0|^2 |\mathbf{G}_0|^2 = \left(\frac{D}{D+1} \right)^2, \quad (7.33)$$

$$v_{\mathbf{G}_0} = v e^{\pm i\pi/(D+1)}, \quad (7.34)$$

$$S_v = -2v \int \frac{d\tau}{\tau_c} \sum_{a=1}^{D+1} \cos\left(2\pi\mathbf{G}_a \cdot \mathbf{r} - \frac{\pi}{D+1}\right), \quad (7.35)$$

$$S_t = -t \int \frac{d\tau}{\tau_c} \sum_{a=1}^{D+1} \left(\frac{\sigma^+}{2} e^{i2\pi\mathbf{R}_a \cdot \mathbf{k}} + H.c. \right). \quad (7.36)$$

In terms of the matrix \mathbf{O} defined in Eq. (4.3), the lattice vectors are explicitly given by

$$\mathbf{G}_a = c(\mathbf{O}_{a1}^{-1}, \mathbf{O}_{a2}^{-1}, \dots, \mathbf{O}_{aD}^{-1}), \quad (7.37)$$

$$\begin{aligned} \mathbf{R}_a &= -\frac{1}{c}(\mathbf{O}_{a1}^{-1}, \mathbf{O}_{a2}^{-1}, \dots, \mathbf{O}_{aD}^{-1}) \\ &= -\frac{\mathbf{G}_a}{c^2} \quad (c = \text{const.}). \end{aligned} \quad (7.38)$$

Note that Eq. (7.35) is identical to the second term in Eq. (4.5) if $N = D + 1$, $n_0 = -1/2$, and $c = 1$. There is a stable intermediate fixed point if $[D/(D + 1)]^2 < |\mathbf{G}_0|^2 < 1$. The results of the ϵ -expansion analysis are summarized in Tables I and II.

Quite interestingly, the phase diagrams for $D \leq 3$ [Fig. 8(a),(b)] and for $D \geq 4$ [Fig. 8(c)] have quite different structures. Unlike for $D = 2$ or 3 , the fixed-point line for $D \geq 4$ approaches the top line from right. Consequently, arbitrarily close to the top line, the intermediate fixed points are *unstable*. As schematically shown in Fig. 8(c), we conjecture that the fixed-point line eventually curves back at a certain critical point ξ and gets continuously connected to the bottom line. Unfortunately, this critical point is not perturbatively accessible, so a definitive evidence to prove (or disprove) the above conjecture is currently not available. In the next subsection, however, we present an argument that supports the conjecture, by using an analysis on a distorted diamond lattice. For this exotic model, the direction from which the intermediate fixed-point line approaches the top line changes *continuously* from right to left as the lattice is deformed. Thus, if the fixed-point line is to be smoothly connected to the bottom line for $D \leq 3$, it is very likely that it will also be the case for $D \geq 4$ despite the difference, because the different feature (the approaching angle) is continuously deformable. In short, the above conjecture is no less reasonable for $D \geq 4$ than for $D \leq 3$. As shown in Fig. 8(c), if $1 < |\mathbf{G}_0|^2 < \xi$, the free fixed point and one of the two intermediate fixed points are both stable. A first order phase transition between the free and the intermediate phases occurs at $T = 0$ as v or t is tuned.

D. Distorted diamond lattice

In this section, we will deform a diamond lattice in a continuous manner to see how the angle with which the intermediate fixed line approaches the free fixed-point line changes. A distorted diamond lattice is defined by the minima of the potential

$$V = -2\frac{v}{\tau_c} \sum_{a=1}^4 \cos\left(2\pi\mathbf{G}_a \cdot \mathbf{r} - \frac{\pi}{4}\right), \quad (7.39)$$

where

$$\begin{aligned} \mathbf{G}_1 &= c(\alpha, 1, 1), \\ \mathbf{G}_2 &= c(\alpha, -1, -1), \\ \mathbf{G}_3 &= c(-\alpha, 1, -1), \\ \mathbf{G}_4 &= c(-\alpha, -1, 1), \quad (c, \alpha = \text{const.}). \end{aligned} \quad (7.40)$$

This lattice is obtained by stretching (or compressing) a diamond lattice in the (100) direction. The regular diamond lattice is restored when $\alpha = 1$.

One of the shortest displacement vectors connecting the two sublattices is

$$\mathbf{R}_1 = -\frac{1}{4c} \left(\frac{1}{\alpha}, 1, 1\right). \quad (7.41)$$

Thus, the relation between the lengths of the shortest direct and reciprocal lattice vectors may be written

$$|\mathbf{G}_0|^2 |\mathbf{R}_0|^2 = \frac{(\alpha^2 + 2)(2\alpha^2 + 1)}{16\alpha^2}. \quad (7.42)$$

If $(11 - \sqrt{105})/4 < \alpha^2 < (11 + \sqrt{105})/4$, then $|\mathbf{G}_0|^2 |\mathbf{R}_0|^2 < 1$ and both trivial fixed points are unstable. Using a similar ϵ -expansion calculation as in the previous subsection, it is straightforward to see that there is a stable intermediate fixed point at $|\mathbf{R}_0|^2 = 1 - \epsilon$ near the localized fixed point ($\epsilon > 0$). The derivation of a flow equation at $|\mathbf{G}_0|^2 = 1 - \epsilon$ for small v is more complicated, but it may be eventually written as

$$\frac{dv}{d\ell} = \epsilon v - f(\alpha)v^3. \quad (7.43)$$

The function $f(\alpha)$ is computed numerically. If $\alpha < 1.9073$, then $f(\alpha) > 0$ and the solution to the above equation exists only if $\epsilon > 0$. The intermediate fixed points are stable and approach the top line from left, as is the case for a regular diamond lattice [Fig. 8(b)]. On the other hand, if $\alpha > 1.9073$, then $f(\alpha) < 0$ and the solution exists only if $\epsilon > 0$. The fixed points are now unstable and approach the top line from right. Consequently, the phase diagram resembles that of a four or higher dimensional honeycomb lattice [Fig. 8(c)]. Since $f(\alpha)$ is a continuous function, the angle with which the fixed-point line approaches the top line is also continuous. Therefore, we come to the following conclusion: If our conjecture in the previous subsection, that the two trivial fixed-point lines are connected by a single intermediate fixed-point line, is correct for $D \leq 3$, it is most likely correct for $D \geq 4$, too, even though the intermediate fixed-point line has a different shape in the two cases.

E. Distorted honeycomb lattice: resonant tunneling of a spin-1/2 Luttinger liquid

As argued in Sec. V, the double-barrier resonant tunneling model of spin-1/2 Luttinger liquid is mapped to the distorted honeycomb lattice. Following Ref. 18, we will briefly discuss the intermediate fixed point of this exotic lattice problem.

Since all v 's in Eq. (5.12) are marginal if $g_\rho = 1$ and $g_\sigma = 3$, one can perform a perturbative renormalization group analysis at $g_\rho = 1 - \epsilon_\rho$ and $g_\sigma = 3 - \epsilon_\sigma$, for small positive ϵ 's. According to Ref. 18, there is a stable intermediate fixed point at $v_e^* = \sqrt{\epsilon_\rho(\epsilon_\rho + \epsilon_\sigma)}$, $v_1^* = (\epsilon_\rho + \epsilon_\sigma)/4$, and $v_2^* = 0$. The renormalization group flow diagram is schematically drawn in Fig. 9 in the v_e - v_1 plane, assuming $v_2 = 0$. This intermediate fixed point is a continuation of that of the regular honeycomb lattice. However, unlike the regular honeycomb lattice, which is described by only one parameter v , there are now three parameters. Since the intermediate fixed point is stable only in one direction, in order to obtain resonance, one has to tune not only one, but two parameters, for example, v_2 and v_e/v_1 .

VIII. MULTICHANNEL KONDO PROBLEM

In this section, we will explicitly derive the mapping between the multichannel Kondo model and the QBM model. Then using the mapping, we will exactly calculate the mobility μ^* at the intermediate fixed point.

In the absence of a magnetic field, the Hamiltonian of the N -channel Kondo model is given by^{32,33}

$$H = H_0 + H_J, \quad (8.1)$$

where

$$H_0 = iv_F \sum_{a,s} \int dx \psi_{as}^\dagger \partial_x \psi_{as}, \quad (8.2)$$

$$H_J = 2\pi v_F \sum_a \left\{ J_z S_{\text{imp}}^z s_a^z(0) + \frac{1}{2} J_\perp \left[S_{\text{imp}}^+ s_a^-(0) + \text{H.c.} \right] \right\}. \quad (8.3)$$

The first term H_0 is the kinetic energy of electrons and H_J is the exchange coupling between the impurity spin \vec{S}_{imp} and the sum of electron spins $\sum_a \vec{s}_a = \sum_a \psi_{as}^\dagger (\vec{\sigma}_{ss'}/2) \psi_{as'}$ at $x = 0$. $\vec{\sigma}$ is the Pauli matrix and a and s are channel and spin indices, respectively. For generality, we assume J_z and J_\perp are independent. Following Emery and Kivelson,³² we bosonize the electron operators

$$\psi_{as} = \frac{1}{\sqrt{2\pi v_F \tau_c}} e^{-i\phi_{as}}, \quad (8.4)$$

where v_F is the Fermi velocity, τ_c is the short-time cutoff, and ϕ_{as} is a boson field that satisfies the following commutation relation

$$[\phi_{as}(x), \phi_{a's'}(x')] = -i\pi \delta_{aa'} \delta_{ss'} \text{sgn}(x - x'). \quad (8.5)$$

If we separate spin $\phi_a^\sigma = \phi_{a\uparrow} - \phi_{a\downarrow}$ from charge $\phi_a^\rho = \phi_{a\uparrow} + \phi_{a\downarrow}$, we may write \vec{s}_a as

$$s_a^z = \frac{1}{4\pi} \partial_x \phi_a^\sigma, \quad (8.6)$$

$$s_a^\pm = \frac{1}{2\pi v_F \tau_c} e^{\pm i \phi_a^\sigma}. \quad (8.7)$$

In the boson representation, the Kondo Hamiltonian is written as

$$H_0 = \sum_{a=1}^N \frac{v_F}{8\pi} \int dx \left[(\partial_x \phi_a^\rho)^2 + (\partial_x \phi_a^\sigma)^2 \right], \quad (8.8)$$

$$H_J = \frac{1}{2} \sum_{a=1}^N \left\{ v_F J_z S_{\text{imp}}^z \partial_x \phi_a^\sigma(0) + \frac{J_\perp}{\tau_c} \left[S_{\text{imp}}^+ e^{-i \phi_a^\sigma(0)} + \text{H.c.} \right] \right\}. \quad (8.9)$$

Since ϕ_a^ρ is free and non-interacting, we will drop it from now on.

The first term in Eq. (8.9) may be eliminated by introducing a unitary transformation

$$U_\lambda = e^{i\lambda S_{\text{imp}}^z \sum_a \phi_a^\sigma(0)}, \quad (8.10)$$

which rotates the axes of the spin space at $x = 0$. The Hamiltonian transforms as

$$H' = U H U^{-1} \quad (8.11)$$

$$= \sum_a \left\{ \frac{v_F}{8\pi} \int dx (\partial_x \phi_a^\sigma)^2 + v_F \left(\frac{J_z}{2} - \lambda \right) S_{\text{imp}}^z \partial_x \phi_a^\sigma(0) + \frac{J_\perp}{2\tau_c} \left[S_{\text{imp}}^+ e^{-i[\phi_a^\sigma(0) - \lambda \sum_b \phi_b^\sigma(0)]} + \text{H.c.} \right] \right\}. \quad (8.12)$$

Now, we set $\lambda = J_z/2$ so that the second term above vanishes. A similar technique has been used in Ref. 32 for the two-channel Kondo problem and in Ref. 36 for the four-channel problem.

For later convenience, we make change of variables using the the same orthogonal transformation \mathbf{O} as in Eq. (4.3):

$$\begin{bmatrix} \phi_i^{\text{sf}} \\ \phi^s \end{bmatrix} = \mathbf{O} \begin{bmatrix} \phi_a^\sigma \end{bmatrix}, \quad (i = 1 \cdots N-1). \quad (8.13)$$

The last component of the left-hand side, $\phi^s = \sum_a \phi_a^\sigma / \sqrt{N}$ is proportional to the sum of the spins in all channels, whereas the other components ϕ_i^{sf} ($i = 1, \dots, N-1$) are ‘‘spin flavors’’. In terms of these new variables, the above Hamiltonian finally becomes

$$H' = \frac{v_F}{8\pi} \int dx \left[(\partial_x \phi^s)^2 + \sum_{i=1}^{N-1} (\partial_x \phi_i^{\text{sf}})^2 \right] + \frac{J_\perp}{2\tau_c} \sum_{a=1}^N \left\{ S_{\text{imp}}^+ e^{-i \left[\frac{1}{\sqrt{N}} (1 - \frac{N}{2} J_z) \phi^s(0) + \sum_{i=1}^{N-1} \mathbf{O}_{ai}^{-1} \phi_i^{\text{sf}}(0) \right]} + \text{H.c.} \right\}. \quad (8.14)$$

Note that there is a reflection symmetry about $J_z = 2/N$. More specifically, H' is invariant under $\phi^s \rightarrow -\phi^s$ and $J_z \rightarrow -J_z + 4/N$. At the symmetry point $J_z = 2/N$, the total spin ϕ^s gets completely decoupled and becomes non-interacting. This is the multichannel generalization of the Toulouse limit of the single-channel model¹³ or the Emery-Kivelson line of the two-channel model.³² Although this special limit is solved exactly for $N \leq 2$, it is not the case for $N \geq 3$. As will be shown later, however, there is a stable fixed point in the Toulouse limit, so some of the low-energy properties may be understood via a renormalization group analysis. This fixed point is identical to the stable intermediate fixed point of the QBM model on an $(N-1)$ -dimensional honeycomb lattice with $|\mathbf{G}_0|^2 = (N-1)/N$.

Now we may obtain the QBM action using the same technique that we have used for the multi-lead quantum dot model. By setting $J_z = 2/N$ and integrating out all degrees of freedom away from $x = 0$, we get

$$S_{\text{Kondo}} = \frac{1}{8\pi^2} \int d\omega |\omega| \sum_{i=1}^N |\phi_i^{\text{sf}}(\omega)|^2 + \frac{J_\perp}{2} \int \frac{d\tau}{\tau_c} \sum_{a=1}^N \left[S_{\text{imp}}^+ e^{-i \sum_{i=1}^{N-1} \mathbf{O}_{ai}^{-1} \phi_i^{\text{sf}}(0)} + \text{c.c.} \right]. \quad (8.15)$$

The above action has *identically* the same form as the multi-dimensional honeycomb lattice model in Eqs. (6.11), (7.36), and (7.38), with $c = 1$. The mapping becomes complete if we make the following substitutions:

$$N \leftrightarrow D + 1, \quad (8.16)$$

$$\phi_i^{\text{sf}}(x=0) \leftrightarrow 2\pi k_i, \quad (8.17)$$

$$J_\perp \leftrightarrow 2t, \quad (8.18)$$

$$S_{\text{imp}}^\pm \leftrightarrow \sigma^\pm / 2, \quad (8.19)$$

$$\mathbf{O}_{ai}^{-1} \leftrightarrow \mathbf{R}_0. \quad (8.20)$$

This mapping may also be understood using the “spin configuration lattice”, just as we have used lattices in $Q_1 - Q_2 - \dots - Q_N$ space for the quantum dot problems. The spin configuration lattice lives in a space where each axis represents the total spin in channel a ,

$$S_a^z = \int dx s_a^z(x). \quad (8.21)$$

For small coupling J_\perp , the change in S_a^z will occur in a step-like manner with unit step height ($\Delta S_a^z = 1$). For the N -channel model, therefore the vectors (S_1^z, S_2^z, \dots) form an N -dimensional cubic lattice with lattice constant $a = 1$. In this lattice, a spin transfer between channels is represented by tunneling of a fictitious particle between lattice sites. The conservation condition of the total electron spin *plus* the impurity spin gives a constraint in the lattice space. Explicitly, the constraint may be written as

$$\sum_a S_a^z = \text{const.} - S_{\text{imp}}^z. \quad (8.22)$$

This is an equation that defines an $(N - 1)$ -dimensional hyper-plane perpendicular to $(11 \dots 1)$ direction. Since $S_{\text{imp}}^z = \pm 1/2$, the fictitious particle is allowed to reside on two adjoining hyper-planes that satisfy the above condition. For the three-channel Kondo model, the two (111) planes are analogous to those shown in Fig. 4(b). In the Toulouse limit ($J_z = 2/N$), the motion perpendicular to the planes gets renormalized at low temperatures and the two planes eventually collapse onto each other at $T = 0$. As a result, we end up with a new tunneling problem in a single plane. In the three-channel case, the resulting lattice is a 2D honeycomb lattice [Fig. 4(b)]. In general, the N -channel Kondo problem in the Toulouse limit is mapped to an $(N - 1)$ -dimensional honeycomb lattice QBM model.

A renormalization group analysis similar to that of Anderson, Yuval, and Hamann³⁷ may be performed to obtain the flow diagram of the multichannel Kondo problem. Details of the calculations are given in Appendix B and we will only present the result here:

$$\frac{dJ_z}{d\ell} = J_\perp^2 \left(1 - \frac{N}{2} J_z\right), \quad (8.23)$$

$$\frac{dJ_\perp}{d\ell} = J_z J_\perp \left(1 - \frac{N}{4} J_z\right) - \frac{N}{4} J_\perp^3. \quad (8.24)$$

The above equations are exact in J_z and perturbative in J_\perp . It is also exact in N , except for the last term in Eq. (8.24), in which we kept only the leading order term in $1/N$. The renormalization flow diagram is schematically drawn in Fig. 10. Obviously, the multichannel Kondo fixed point lies on the Toulouse line $J_z = 2/N$. Although it is a highly non-trivial strong coupling fixed point, we may use known results of the conformal field theory to exactly compute some physical quantities. On the other hand, we may use the mapping to the QBM model and perturbatively access the fixed point in the large D limit of the D -dimensional honeycomb lattice model. Therefore, it is possible to directly compare the two results, in order to test the mapping and the perturbative analysis of the QBM model in a non-trivial way. Specifically, we will calculate below the scaling dimension of the leading irrelevant operator Δ and the fixed point mobility μ^* using both methods.

From a conformal field theory calculation, the scaling dimension of the leading irrelevant operator at the Kondo fixed point is given by³³

$$\Delta = 1 + \frac{2}{N + 2}. \quad (8.25)$$

We may also compute the same quantity using an ϵ -expansion technique described in Appendix C. By substituting $N = D + 1$ in Eq. (C15), we get

$$\Delta = 1 + \frac{2}{N} - \frac{4}{N^2} + \mathcal{O}\left(\frac{1}{N^3}\right). \quad (8.26)$$

This obviously agrees with Eq. (8.25) for large N .

The next quantity we compute is the universal mobility μ^* of the QBM model at the intermediate fixed point. Firstly, we use the conformal field theory results of the Kondo model. Let us define the spin currents

$$J_a = v_F s_a^z \quad (8.27)$$

$$= \frac{v_F}{4\pi} \partial_x \phi_a = \frac{1}{4\pi} \partial_t \phi_a, \quad (8.28)$$

and their linear combinations

$$J^s = \sum_a \frac{1}{\sqrt{N}} J_a = \frac{1}{4\pi} \partial_t \phi^s, \quad (8.29)$$

$$J_i^{\text{sf}} = \sum_a O_{ia} J_a = \frac{1}{4\pi} \partial_t \phi_i^{\text{sf}}. \quad (8.30)$$

Note that J^s is the total spin current and J_i^{sf} are the spin flavor currents. Since the analogue of the Brownian particle position r_i is the total spin flavor in each channel $S_i^{\text{sf}} = \sum_a O_{ia} S_a^z$, the velocity $\partial_t r_i$ is mapped to the rate in which spin flavor is “injected” into channel i . Since the injection occurs at $x = 0$ through the exchange coupling H_J , the spin flavor injection rate $\partial_t S_i^{\text{sf}}$ may be measured via the difference in J_i^{sf} right before and after $x = 0$. In other words, we have a one-to-one correspondence

$$J_i^{\text{sf}}(x = 0^+) - J_i^{\text{sf}}(x = 0^-) \leftrightarrow \partial_t r_i. \quad (8.31)$$

From the above mapping and Eq. (6.7), we get

$$\mu = \lim_{\omega \rightarrow 0} \frac{1}{2\pi|\omega|} \int d\tau (1 - e^{i\omega\tau}) \left\langle \text{T}_\tau [J_i^{\text{sf}}(0^+, \tau) - J_i^{\text{sf}}(0^-, \tau)] [J_i^{\text{sf}}(0^+, 0) - J_i^{\text{sf}}(0^-, 0)] \right\rangle_0, \quad (8.32)$$

where T_τ is the time ordering operator and the average $\langle \dots \rangle_0$ is calculated with respect to the free non-interacting Hamiltonian H_0 . The above fixed point correlation functions have been exactly calculated by Ludwig and Affleck^{38,39} using conformal field theory. Specifically, they are given by

$$\langle \text{T}_\tau J_i^{\text{sf}}(0^+, \tau) J_i^{\text{sf}}(0^+, 0) \rangle_0 = \langle \text{T}_\tau J_i^{\text{sf}}(0^-, \tau) J_i^{\text{sf}}(0^-, 0) \rangle_0 = \frac{1}{2\tau^2}, \quad (8.33)$$

$$\langle \text{T}_\tau J_i^{\text{sf}}(0^+, \tau) J_i^{\text{sf}}(0^-, 0) \rangle_0 = \langle \text{T}_\tau J_i^{\text{sf}}(0^-, \tau) J_i^{\text{sf}}(0^+, 0) \rangle_0 = \frac{a_J^K}{2\tau^2}, \quad (8.34)$$

where

$$a_J^K = \frac{S_{1/2}^1/S_0^1}{S_{1/2}^0/S_0^0} \quad (8.35)$$

and the “modular S-matrix” is given by

$$S_{j'}^j = \sqrt{\frac{2}{N+2}} \sin \left[\frac{\pi(2j+1)(2j'+1)}{N+2} \right]. \quad (8.36)$$

Thus, Eq. (8.32) becomes

$$\mu^* = \frac{1 - a_J^K}{2} \quad (8.37)$$

$$= 2 \sin^2 \frac{\pi}{N+2}. \quad (8.38)$$

This result agrees with Emery and Kivelson³² for $N = 2$, where it takes the perfect value $\mu^* = 1$ [See also Sec. III].

The perturbation calculation of μ^* in the large D limit of the QBM model is described in Appendix C. The result is given by

$$\mu^* = 2\pi^2 \left(\frac{1}{N^2} - \frac{4}{N^3} \right) + \mathcal{O} \left(\frac{1}{N^4} \right). \quad (8.39)$$

It agrees with Eq. (8.38) for large N .

IX. ON-RESONANCE CONDUCTANCE AND THE UNIVERSAL SCALING

In this section, we will compute the on-resonance conductance of the two-lead spin-1/2 quantum dot model⁶ using the mapping of the quantum dot model to both the Kondo problem and the QBM model. For convenience, we will actually consider a four-lead spinless model instead of the spin-1/2 model, since they are equivalent (see Sec. II).

First of all, we define the conductance matrix for an N -lead model

$$G_{ab} = \lim_{V_1, V_2, \dots, V_N \rightarrow 0} \frac{\partial}{\partial V_b} \langle -e \partial_t Q_a \rangle. \quad (9.1)$$

It characterizes the linear current flowing *into* the a -th lead in response to an infinitesimal voltage V_b in the b -th lead. The mapping described in the previous sections dictates that the current and the voltage are mapped to the spin current and the local channel magnetic field in a Kondo model, respectively. Thus, we may alternatively compute the “spin conductance” of the Kondo model. Explicitly, it is defined as

$$G_{ab} = -\frac{e^2}{h} \lim_{\omega \rightarrow 0} \frac{1}{2\pi|\omega|} \int d\tau (1 - e^{i\omega\tau}) \langle \mathbf{T}_\tau [J_a(0^+, \tau) - J_a(0^-, \tau)] [J_b(0^+, 0) - J_b(0^-, 0)] \rangle, \quad (9.2)$$

where the spin current in each Kondo channel J_a is defined in Eq. (8.27). Using Eqs. (8.30) and (8.32), the above equation may be evaluated to yield

$$G_{ab} = \frac{e^2}{h} \left(\frac{1}{N} - \delta_{ab} \right) \mu, \quad (9.3)$$

where μ is the mobility of the corresponding QBM model.

A four-lead model is equivalent to the two-lead spin-1/2 model if we map the lead 1 and 2 (3 and 4) to the two spin channels of the source (drain) lead. If we apply an infinitesimal voltage V to the source relative to the drain, i.e.,

$$V_a = \begin{cases} V & \text{if } a = 1, 2, \\ 0 & \text{if } a = 3, 4, \end{cases} \quad (9.4)$$

then the current is given by

$$I = \sum_{a=3}^4 \langle -e \partial_t Q_a \rangle \quad (9.5)$$

$$= \sum_{a=3}^4 \sum_{b=1}^4 G_{ab} V_b \quad (9.6)$$

$$= \mu \frac{e^2}{h} V. \quad (9.7)$$

Substituting the on-resonance mobility $\mu^* = 1/2$ in Eq. (8.38) to the above equation, we get

$$G^* = \mu^* \frac{e^2}{h} = \frac{e^2}{2h}. \quad (9.8)$$

Physically, this result may be understood as follows: On resonance at $T = 0$, the conductance of each QPC is given by $2\mu^* e^2/h = e^2/h$, where there is an overall factor of two due to spin. Then the above G^* is the series conductance of the two QPCs (see Sec. II).

Experimentally, G^* may be measured as the peak value of a conductance resonance as one sweeps the gate voltage. Again, the shape of the peak follows a scaling function that is independent of microscopic details of the system. Since the scaling dimension of the magnetic field \mathcal{H} is given by $1/3$,³³ the resonance line shape has the form

$$G(\delta n_0, T) = \tilde{G} \left(\frac{\delta n_0}{T^{2/3}} \right). \quad (9.9)$$

In principle, the explicit form of \tilde{G} may be obtained using a Monte Carlo simulation.⁴⁰

X. CONCLUSIONS

In this paper, we have used a QBM model with periodic potential to study a few different fundamental problems in condensed matter physics. Generically, by integrating out unimportant degrees of freedom in a path integral representation, one can obtain an alternative description of a problem in terms of a first-quantized quantum mechanical model of a single Brownian particle moving in a periodic potential. The remaining degrees of freedom are mapped to the spatial coordinates of the Brownian particle, whereas the integrated ones serve as the source of dissipation.

We have applied this method to such problems as resonant tunneling in quantum dot and Luttinger liquid systems as well as multichannel Kondo problems. For an N -lead quantum dot model in the limit $\Delta E \ll T \ll e^2/C$, we have shown that the on-resonance problem is mapped to an $(N - 1)$ -dimensional honeycomb lattice and the off-resonance problem to an $(N - 1)$ -dimensional triangular lattice. Each vector component of the Brownian particle position is the total charge in each lead, and the periodic potential comes from backscattering. Analogously, by mapping the total spin in each channel to each vector component of the position, we could derive similar mappings for the N -channel Kondo problem in the Toulouse limit.

The lattice symmetry of the periodic potential determines the zero-temperature phase diagram. For symmorphic lattices, there are two trivial zero-temperature phases: If the dissipation is strong or the lattice sites are far apart, the Brownian particle gets localized and the mobility μ vanishes. If the dissipation is weak or the lattices sites are close to one another, the particle diffuses freely and the mobility takes its perfect maximum value $\mu = 1$. We have analyzed the phase diagrams in perturbatively accessible regimes.

For non-symmorphic lattices, the extra symmetry between sublattices may give rise to an intermediate phase. The mobility in this phase is given a universal value in the range $0 < \mu < 1$ and independent of the microscopic details of the problem. The intermediate phase is governed by the multichannel Kondo fixed point. We have explicitly demonstrated that the mappings are consistent by computing the scaling dimension of the leading irrelevant operator and the fixed point mobility in both the QBM model and the Kondo model, in the large N limit.

Exploiting the mapping, we have used spin current correlation functions calculated by a conformal field theory to compute the mobility at the intermediate fixed point exactly. Using the result

$$\mu^* = 2 \sin^2 \frac{\pi}{N+2}, \quad (10.1)$$

we could also calculate the on-resonance linear conductance G_{ab} between each individual lead for the N -lead quantum dot model. Particularly for the conventional two-lead spin-1/2 model, the on-resonance conductance is given by $G = e^2/2h$. Experimentally, this conductance may be measured from the peak value of the conductance resonance as a function of the gate voltage. From the QBM theory, the resonance line shape is predicted to be described by a scaling function of the form

$$G(\delta n_0, T) = \tilde{G} \left(\frac{\delta n_0}{T^\alpha} \right). \quad (10.2)$$

where α is determined from the scaling dimension of the local magnetic field at the magnetic impurity. Specifically, $\alpha = 2/3$ for the two-lead spin-1/2 quantum dot model and $\alpha = 1/2$ for the spinless model.

ACKNOWLEDGMENTS

It is a pleasure to thank C. L. Kane for invaluable discussions and comments. K. A. Matveev, J. J. Palacios, and T. S. Kim are also acknowledged for useful discussions. This work has been supported by NSF under grant DMR-98-70681.

APPENDIX A: RENORMALIZATION GROUP ANALYSIS OF THE QBM MODEL

In this appendix, we develop a renormalization group analysis method for the QBM model. The renormalization group flow equation for the triangular lattice will be explicitly calculated as an example. More examples can be found in Appendix C for D -dimensional honeycomb lattices in the large D limit.

Let us consider the small v limit of the action as in Eqs. (6.1) through (6.3). It should be straightforward to perform a similar analysis for the small t limit using a dual theory in Eqs. (6.10) through (6.12). The partition function is given by

$$Z = \int \mathcal{D}[\mathbf{r}(\tau)] e^{-S_0[\mathbf{r}] - S_v[\mathbf{r}]} \quad (\text{A1})$$

$$= Z_0 \sum_n \frac{1}{n!} \langle (-S_v)^n \rangle. \quad (\text{A2})$$

where $Z_0 = \int \mathcal{D}[\mathbf{r}] e^{-S_0}$ is the the partition function for $v = 0$. The brackets denote an average with respect to the free action S_0 and are defined as

$$\langle O \rangle \equiv \frac{1}{Z_0} \int \mathcal{D}[\mathbf{r}] O e^{-S_0}. \quad (\text{A3})$$

Each term in Eq. (A2) may be explicitly written as

$$\frac{1}{n!} \langle (-S_v)^n \rangle = \sum_{\{\mathbf{G}\}} \int_{\tau_1 < \tau_2 < \dots < \tau_n} \left(\prod_i \frac{d\tau_i}{\tau_c} v_i \right) \langle e^{i2\pi \sum_i \mathbf{G}_i \cdot \mathbf{r}(\tau_i)} \rangle, \quad (\text{A4})$$

where v_i is a shorthand notation for $v_{\mathbf{G}_i}$. The prefactor $1/n!$ has been absorbed in the explicit time ordering. For a non-symmorphic lattice, time ordering is important because the Brownian particle has to move back and forth between different sublattices. An explicit calculation at $T = 0$ shows that

$$\langle e^{i2\pi \sum_i \mathbf{G}_i \cdot \mathbf{r}(\tau_i)} \rangle = \begin{cases} \prod_{i < j} \left[\frac{\tau_c^2}{(\tau_j - \tau_i)^2 + \tau_c^2} \right]^{-\mathbf{G}_i \cdot \mathbf{G}_j} & \text{if } \sum \mathbf{G}_i = 0, \\ 0 & \text{otherwise.} \end{cases} \quad (\text{A5})$$

Any low energy properties calculated from the above partition function must not depend on the cutoff τ_c . Therefore, by renormalizing τ_c , we may obtain a set of scaling laws that connect a given problem to another one with renormalized parameters. In the new theory with cutoff $\tau'_c = \tau_c e^\ell$, we may define the renormalized amplitude v_i^R in such a way that Eq. (A2) retains the same form when written in terms of v_i^R and τ'_c . With the help of Eq. (A5), this condition may be written as

$$\left(\frac{v_i^R}{\tau_c e^\ell} \right)^2 \left[\frac{(\tau_c e^\ell)^2}{(\tau_2 - \tau_1)^2 + (\tau_c e^\ell)^2} \right]^{|\mathbf{G}_i|^2} = \left(\frac{v_i}{\tau_c} \right)^2 \left[\frac{\tau_c^2}{(\tau_2 - \tau_1)^2 + \tau_c^2} \right]^{|\mathbf{G}_i|^2}, \quad (\text{A6})$$

to the second order in v . Assuming $\tau_c \ll \tau_c e^\ell \ll \tau_2 - \tau_1$, we get a simple scaling equation

$$v_i^R e^{(|\mathbf{G}_i|^2 - 1)\ell} = v_i. \quad (\text{A7})$$

Differentiating both sides of Eq. (A7) with respect to ℓ , we obtain the renormalization group flow equation (6.9).

Higher order corrections may be calculated in a similar way. Let us consider any arbitrary pair of consecutive operators at time τ_i and τ_{i+1} in Eq. (A4). If $\tau_c < \tau_{i+1} - \tau_i < \tau_c e^\ell$, they are no longer distinguished in the new theory with cutoff $\tau_c e^\ell$. Instead, they must be treated as a compound operator at a single moment:

$$e^{i2\pi \mathbf{G}_i \cdot \mathbf{r}(\tau_i)} e^{i2\pi \mathbf{G}_{i+1} \cdot \mathbf{r}(\tau_{i+1})} \rightarrow e^{i2\pi (\mathbf{G}_i + \mathbf{G}_{i+1}) \cdot \mathbf{r}(\tau_i)}. \quad (\text{A8})$$

This gives rise to the second order correction to Eq. (A7). This process may be thought of as ‘‘decimation’’ of closely placed operator sequences in time. In general, we get the n -th order correction by lumping together n operators that lie within $\tau_c e^\ell$.

In order to show details of the decimation procedure, we will consider a triangular lattice as a specific example. The shortest reciprocal lattice vectors \mathbf{G}_i and $-\mathbf{G}_i$ ($i = 1, 2, 3$) are defined as in Fig. 7(a). We need to find all \mathbf{G} -sequences that add up to a single reciprocal lattice vector. For example, since $\mathbf{G}_1 + \mathbf{G}_2 + \mathbf{G}_3 = 0$, there are two sequences that are second order in v :

$$\{-\mathbf{G}_2, -\mathbf{G}_3\}, \{-\mathbf{G}_3, -\mathbf{G}_2\}, \quad (\text{A9})$$

that add up to \mathbf{G}_1 . When decimated, they give rise to a correction to the righthand side of Eq. (A7)

$$(\zeta_{\{\overline{23}\}} + \zeta_{\{\overline{32}\}}) v^2, \quad (\text{A10})$$

where

$$\zeta_{\{\overline{23}\}} = \int_0^{\tau_c e^\ell} \frac{d\tau'}{\tau_c} \left\langle e^{i2\pi[-\mathbf{G}_2 \cdot \mathbf{r}(\tau_1) - \mathbf{G}_3 \cdot \mathbf{r}(\tau_1 + \tau') - \mathbf{G}_1 \cdot \mathbf{r}(\tau_2)]} \right\rangle_{\tau_c} \left/ \left(\frac{\tau_c}{\tau_2 - \tau_1} \right)^{2|\mathbf{G}_1|^2} \right., \quad (\text{A11})$$

$$\zeta_{\{\overline{32}\}} = \int_0^{\tau_c e^\ell} \frac{d\tau'}{\tau_c} \left\langle e^{i2\pi[-\mathbf{G}_3 \cdot \mathbf{r}(\tau_1) - \mathbf{G}_2 \cdot \mathbf{r}(\tau_1 + \tau') - \mathbf{G}_1 \cdot \mathbf{r}(\tau_2)]} \right\rangle_{\tau_c} \left/ \left(\frac{\tau_c}{\tau_2 - \tau_1} \right)^{2|\mathbf{G}_1|^2} \right.. \quad (\text{A12})$$

Each of the above terms comes from the corresponding sequence in Eq. (A9). We have assumed $v_1 = v_2 = v_3 = v$. The overlines in $\overline{2}$ and $\overline{3}$ denote that the corresponding vectors have a minus sign. In general, it is not easy to compute ζ , but if $|\mathbf{G}_i|^2 \approx 1$, we get

$$\zeta_{\{\overline{23}\}} = \zeta_{\{\overline{32}\}} = \ell. \quad (\text{A13})$$

Thus the scaling equation becomes

$$v^R e^{(|\mathbf{G}_i|^2 - 1)\ell} = v + 2\ell v^2. \quad (\text{A14})$$

By differentiating both sides of Eq. (A14) with respect to ℓ and writing the final equation in terms of the renormalized parameter v^R , we obtain the renormalization group flow equation. For $|\mathbf{G}_i|^2 = 1 + \epsilon$, it becomes Eq. (7.10).

This analysis may be straightforwardly generalized to even higher order corrections and nonidentical v 's. In general, for every sequence $\{\mathbf{G}_{i_1}, \dots, \mathbf{G}_{i_n}\}$ such that $\sum_p \mathbf{G}_{i_p} = \mathbf{G}_1$, there is an n -th order contribution

$$\zeta_{\{i_1 i_2 \dots i_n\}} v_{i_1} v_{i_2} \dots v_{i_n} \quad (\text{A15})$$

to the righthand side of Eqs. (A7) and (A14), where

$$\zeta_{\{i_1 i_2 \dots i_n\}} = \int_{0 < \tau_2 < \tau_3 < \dots < \tau_n < \tau_c e^\ell} \left(\prod_{p=2}^n \frac{d\tau_p}{\tau_c} \right) \prod_{1 \leq p < q \leq n} \left[\frac{\tau_c^2}{(\tau_q - \tau_p)^2 + \tau_c^2} \right]^{-\mathbf{G}_{i_p} \cdot \mathbf{G}_{i_q}}. \quad (\text{A16})$$

It is assumed that $\tau_1 = 0$ in the above integrand. For the two-vector sequences in Eq. (A9), disconnected terms identically vanished up to the second order. In general, however, they are finite and have to be carefully taken care of. Disconnected terms can be treated basically in the same way as above, except for that they are products of one non-loop and one or more loops, where a loop is a subgroup of sequences that add up to zero. For example, there is a fourth order disconnected sequence $\{\mathbf{G}_1\}\{\mathbf{G}_1, \mathbf{G}_2, \mathbf{G}_3\}$. The first subgroup trivially adds up to \mathbf{G}_1 , but the second subgroup is a loop [Fig. 7(b)]. The contribution from this process is given by

$$\zeta_{\{1\}} \zeta_{\{123\}} v_1^2 v_2 v_3, \quad (\text{A17})$$

where we define $\zeta_{\{i\}} = 1$. Higher order calculations for a D -dimensional honeycomb lattice in the large D limit is given in Appendix C.

APPENDIX B: RENORMALIZATION GROUP ANALYSIS OF THE MULTICHANNEL KONDO PROBLEM

In this appendix, we derive the flow equations (8.23) and (8.24) of the multichannel Kondo model. In the boson representation, the partition function may be written as

$$Z = \int \mathcal{D}[\phi^s, \phi_i^{\text{sf}}] e^{-\int d\tau H'}, \quad (\text{B1})$$

where H' is the Hamiltonian given in Eq. (8.14). For small J_\perp , we may write it in a Taylor series expansion as

$$Z = Z_0 \sum_n \frac{1}{n!} \left(\frac{J_\perp}{2} \right)^n \left\langle \left\{ \int \frac{d\tau}{\tau_c} \sum_{a=1}^N \left[S_{\text{imp}}^+ e^{-i(K\phi^s + \sum_i \text{O}_{ai}^{-1} \phi_i^{\text{sf}})} + \text{c.c.} \right] \right\}^n \right\rangle \quad (\text{B2})$$

$$= Z_0 \sum_n \left(\frac{J_\perp}{2} \right)^n \int_{\tau_1 < \tau_2 < \dots < \tau_n} \prod_{a=1}^N \left(\frac{d\tau_p}{\tau_c} \right) \sum_{\{a_p\}} \left\langle e^{-i \sum_p s_p (K\phi^s + \sum_i \text{O}_{a_p i}^{-1} \phi_i^{\text{sf}})} + \text{c.c.} \right\rangle, \quad (\text{B3})$$

where $K \equiv (1 - NJ_z/2)/\sqrt{N}$ and s_p alternates between ± 1 due to S_{imp}^\pm . The average $\langle \dots \rangle$ and the free partition function Z_0 are calculated for $J_\perp = 0$. After the averages are evaluated, the above equation becomes

$$Z = Z_0 \sum_n \left(\frac{J_\perp}{2}\right)^n \int' \prod_{a=1}^N \left(\frac{d\tau_p}{\tau_c}\right) \sum_{\{a_p\}} e^{-\sum_{p<q} V_{pq}} \delta\left(\sum_p s_p \mathbf{O}_{a_p}^{-1}\right), \quad (\text{B4})$$

where \int' implies integration over the range $\tau_1 < \tau_2 < \dots < \tau_n$, and

$$V_{pq} \equiv -2s_p s_q \left(K^2 + \sum_i \mathbf{O}_{a_p i}^{-1} \mathbf{O}_{i a_q}\right) \ln \frac{\tau_q - \tau_p}{\tau_c}. \quad (\text{B5})$$

It is convenient to view Eq. (B4) as the partition function of a plasma in the τ -space. There are N types of unit charges \mathbf{O}_{ai}^{-1} ($a = 1, \dots, N$). Since each charge is characterized by $N - 1$ vector components ($i = 1, \dots, N - 1$), it is a ‘‘vector plasma’’. An arbitrary single charge in the plasma may be identified by the position τ , the charge type a , and the sign of the charge s . Then, V_{pq} is the interaction energy between two charges (τ_p, a_p, s_p) and (τ_q, a_q, s_q) .

We now analyze this model using a real-space renormalization group method.³⁷ A similar analysis of 1D plasma model has been performed for a Luttinger liquid resonant tunneling problem in Ref. 18, but it differs from our model in that charges in their model are conventional scalar objects. In the first step of the renormalization group transformation, we decimate pairs of closely placed charges. Suppose there is a $\pm \mathbf{O}_{ai}^{-1}$ charge pair at τ' and $\tau' + \Delta\tau$. If $\Delta\tau$ is small compared to the distance between this pair and other charges, the pair may be thought of as a dipole. The total interaction of this dipole and all other charges is given by

$$V_a^{\text{dipole}}(\tau'; \Delta\tau) = -2 \sum_q s_p s_q \left(K^2 + \sum_i \mathbf{O}_{ai}^{-1} \mathbf{O}_{i a_q}\right) \Delta\tau \partial_{\tau'} \ln \frac{|\tau' - \tau_q|}{\tau_c}. \quad (\text{B6})$$

If $\tau_c < \Delta\tau < \tau_c + \delta\tau_c$, the dipole is no longer recognizable after increasing the cutoff from τ_c to $\tau_c + \delta\tau_c$. However, it induces effective interaction of order $\delta\tau_c/\tau_c$ between other charges. When all such dipoles are integrated out, the partition function becomes

$$Z = Z_0 \sum_n \left(\frac{J_\perp}{2}\right)^n \int' \prod_{a=1}^N \left(\frac{d\tau_p}{\tau_c}\right) \sum'_{\{a_p\}} e^{-\sum_{p<q} V_{pq}} \left\{ 1 + \left(\frac{J_\perp}{2}\right)^2 \frac{\delta\tau_c}{\tau_c} \sum_p \int_{\tau_p}^{\tau_{p+1}} \frac{d\tau'}{\tau_c} \sum_a [1 - V_a^{\text{dipole}}(\tau'; \tau_c)] \right\} \quad (\text{B7})$$

$$= Z_0 \sum_n \left(\frac{J_\perp}{2}\right)^n \int' \prod_{a=1}^N \left(\frac{d\tau_p}{\tau_c}\right) \sum'_{\{a_p\}} e^{-\sum_{p<q} V_{pq}} \left\{ 1 + \left(\frac{J_\perp}{2}\right)^2 \frac{\delta\tau_c}{\tau_c} N \left[\frac{1}{T\tau_c} - \sum_{p<q} 8s_p s_q K^2 \ln \frac{\tau_q - \tau_p}{\tau_c} \right] \right\} \quad (\text{B8})$$

$$= Z_0 e^{NJ_z^2 \delta\tau_c / 4T\tau_c^2} \sum_n \left(\frac{J_\perp}{2}\right)^n \int' \prod_{a=1}^N \left(\frac{d\tau_p}{\tau_c}\right) \sum'_{\{a_p\}} \exp \left[- \sum_{p<q} \left(V_{pq} + \frac{2NJ_z^2 \delta\tau_c}{\tau_c} s_p s_q K^2 \ln \frac{\tau_q - \tau_p}{\tau_c} \right) \right]. \quad (\text{B9})$$

The notation $\sum'_{\{a_p\}}$ means that the sum is only over the vectors that form a loop, i.e., $\sum_p s_p \mathbf{O}_{a_p}^{-1} = 0$. We complete the renormalization group transformation by rescaling $\tau \rightarrow \tau e^\ell$ where $\ell = \delta\tau_c/\tau_c$. Comparing the final expression with the original partition function in Eq. (B4), we obtain the renormalization group flow equations

$$\frac{dJ_z}{d\ell} = J_\perp^2 \left(1 - \frac{N}{2} J_z\right), \quad (\text{B10})$$

$$\frac{dJ_\perp}{d\ell} = J_z J_\perp \left(1 - \frac{N}{4} J_z\right), \quad (\text{B11})$$

which are exact in J_z and perturbative in J_\perp . The extra higher order term in Eq. (8.24) has been read off using the mapping between the Kondo model and the QBM model in the limit $N \gg 1$ and $|J_z - 2/N| \ll 1$.

APPENDIX C: PERTURBATIVE CALCULATIONS

This appendix is devoted to the computation of physical quantities at the intermediate fixed point of the D -dimensional honeycomb lattice in the large D limit. In the first subsection, we derive the renormalization group flow equation in the Toulouse limit and perturbatively compute the scaling dimension of the leading irrelevant operator. In the second subsection, we calculate the fixed point mobility to leading and subleading order in $1/D$.

1. Renormalization group flow equations

We use the tunneling part of the action in Eq. (7.28) in the small t limit. The shortest direct lattice vectors of a D -dimensional honeycomb lattice are given in Eq. (7.38). We will continue to use the same convention in which $\mathbf{R}_0 \in \{\mathbf{R}_i\}$ ($\{-\mathbf{R}_i\}$) if it originates from A sublattice (B sublattice). In the Toulouse limit ($c = 1$), they satisfy

$$|\mathbf{R}_0|^2 = \frac{D}{D+1}. \quad (\text{C1})$$

If D is large, $|\mathbf{R}_0|^2 \approx 1$ and t is only slightly relevant. The intermediate fixed point thus lies perturbatively close to the localized fixed point ($t^* \approx 0$). The renormalization group analysis is very similar to that of the small v limit in Appendix A. The leading order scaling equation may be simply read off from Eq. (A7):

$$t^R e^{-\ell/(D+1)} = t. \quad (\text{C2})$$

The next lowest order term is proportional to t^3 and may be computed using a similar renormalization group technique as in Appendix A. There are three third-order sequences that add up to \mathbf{R}_1 :

$$\begin{aligned} & \{\mathbf{R}_1, -\mathbf{R}_1, \mathbf{R}_1\}, \\ & \{\mathbf{R}_1, -\mathbf{R}_i, \mathbf{R}_i\}, \\ & \{\mathbf{R}_i, -\mathbf{R}_i, \mathbf{R}_1\}, \quad (i \neq 1). \end{aligned} \quad (\text{C3})$$

According to Eq. (A15), their contributions to the scaling equation are

$$\zeta_{\{1\bar{1}\bar{1}\}} t^3, \zeta_{\{1\bar{1}i\}} t^3, \zeta_{\{i\bar{1}\bar{1}\}} t^3, \quad (i \neq 1), \quad (\text{C4})$$

respectively. There are also disconnected terms

$$\{\mathbf{R}_1\}\{\mathbf{R}_i, -\mathbf{R}_i\}, \quad (\text{C5})$$

and their contributions are

$$\zeta_{\{1\}} \zeta_{\{i\bar{i}\}}. \quad (\text{C6})$$

Using Eq. (A16), we may explicitly compute the sum of all third order corrections:

$$\zeta_3 = \zeta_{\{1\bar{1}\bar{1}\}} + \sum_{i=2}^{D+1} \left(\zeta_{\{1\bar{1}i\}} + \zeta_{\{i\bar{1}\bar{1}\}} \right) - \sum_{i=1}^{D+1} \zeta_{\{1\}} \zeta_{\{i\bar{i}\}} \quad (\text{C7})$$

$$= 2\ell \int_0^1 dx \left[D \frac{(1-x)^{2/D} - 1}{x^2} + \frac{2}{x} \right]. \quad (\text{C8})$$

In the large D limit,

$$\zeta_3 = -(D+5)\ell + \mathcal{O}(1/D). \quad (\text{C9})$$

In order to obtain results up to the subleading order in $1/D$, we need to calculate the fifth order contribution ζ_5 . A calculation analogous to the above yields

$$\begin{aligned} \zeta_5 &= \zeta_{\{1\bar{1}\bar{1}\bar{1}\bar{1}\}} \\ &+ \sum_{i \geq 2} \left(\zeta_{\{1\bar{1}\bar{1}i\}} + \zeta_{\{1\bar{1}i\bar{1}\}} + \zeta_{\{1i\bar{1}\bar{1}\}} + \zeta_{\{i\bar{1}\bar{1}\bar{1}\}} + \zeta_{\{i\bar{1}\bar{1}i\}} + \zeta_{\{i\bar{1}i\bar{1}\}} \right) \\ &+ \sum_{i \geq 2} \left(\zeta_{\{1i\bar{i}i\}} + \zeta_{\{i\bar{i}i\bar{i}\}} + \zeta_{\{i\bar{i}i\bar{i}\}} \right) \\ &+ \sum_{2 \leq i < j} \left(\zeta_{\{1i\bar{i}j\bar{j}\}} + \zeta_{\{1i\bar{j}j\bar{i}\}} + \zeta_{\{i\bar{i}j\bar{j}\bar{i}\}} + \zeta_{\{i\bar{j}j\bar{i}i\}} + \zeta_{\{i\bar{i}j\bar{j}i\}} + \zeta_{\{i\bar{j}j\bar{i}i\}} \right) \end{aligned}$$

$$\begin{aligned}
& - \left[\zeta_{\{1\bar{1}\bar{1}\}} + \sum_{i \geq 2} \left(\zeta_{\{1\bar{i}\bar{i}\}} + \zeta_{\{i\bar{i}\bar{1}\}} \right) \right] \left[\sum_{i \geq 1} \zeta_{\{i\bar{i}\}} \right] \\
& - \zeta_{\{1\}} \left[\sum_{i \geq 1} \zeta_{\{i\bar{i}\bar{i}\}} + \sum_{1 \leq i < j} \left(\zeta_{\{i\bar{i}j\bar{j}\}} + \zeta_{\{i\bar{j}j\bar{i}\}} \right) \right] \\
& + \zeta_{\{1\}} \left[\sum_{i \geq 1} \zeta_{\{i\bar{i}\}} \right]^2.
\end{aligned} \tag{C10}$$

Collecting only the leading order terms in D , we get

$$\zeta_5 = 2D^2\ell + \mathcal{O}(D). \tag{C11}$$

Combining Eqs. (C2), (C9), and (C11) and differentiating it with respect to ℓ , we obtain the following renormalization group flow equation:

$$\frac{dt^R}{d\ell} = \frac{1}{D+1}t^R - (D+5)(t^R)^3 + 2D^2(t^R)^5. \tag{C12}$$

From $dt/d\ell = 0$, the intermediate fixed point is given by

$$t^* = \frac{1}{D} - \frac{2}{D^2} + \mathcal{O}\left(\frac{1}{D^3}\right). \tag{C13}$$

By substituting $t^R = t^* + \delta t$ in Eq. (C12), we get

$$\frac{d\delta t}{d\ell} = -\frac{2}{D} + \frac{6}{D^2} + \mathcal{O}\left(\frac{1}{D^3}\right). \tag{C14}$$

Therefore, the scaling dimension of the leading irrelevant operator is

$$\Delta = 1 + \frac{2}{D} - \frac{6}{D^2} + \mathcal{O}\left(\frac{1}{D^3}\right). \tag{C15}$$

Since the D -dimensional lattice model is mapped onto the $(D+1)$ -channel Kondo model, we may compare Eq. (C15) with Eq. (8.25) by setting $N = D + 1$. Clearly, they agree with each other.

2. Fixed point mobility

Now we compute the mobility at the intermediate fixed point obtained above. We will first add a source term

$$S_h = \frac{1}{2} \int d\omega |\omega| e^{|\omega|\tau_c} [\mathbf{h}(\omega) \cdot \mathbf{k}(-\omega) + \text{c.c.}], \tag{C16}$$

to the total action. From Eq. (6.13), the mobility may be expressed as

$$\mu = 1 - \lim_{\omega \rightarrow 0} \frac{1}{D|\omega|} \sum_{i=1}^D \int d\omega' \omega \omega' \langle k_i(\omega) k_i(-\omega') \rangle \tag{C17}$$

$$= 1 - \lim_{\mathbf{h}, \omega \rightarrow 0} \frac{1}{D|\omega|} \sum_{i=1}^D \frac{1}{Z} \int d\omega' \omega \omega' \frac{\delta^2 Z}{\delta h_i(-\omega) \delta h_i(\omega')}, \tag{C18}$$

where

$$Z = \int \mathcal{D}[\mathbf{k}(\tau)] e^{-S[\mathbf{k}]} \tag{C19}$$

is the partition function. By shifting the dummy variable

$$\mathbf{k}(\omega) \rightarrow \mathbf{k}(\omega) - \mathbf{h}(\omega), \quad (\text{C20})$$

we may write the action as

$$S = \frac{1}{2} \int d\omega |\omega| e^{|\omega|\tau_c} [|\mathbf{k}(\omega)|^2 + |\mathbf{h}(\omega)|^2] - t \int \frac{d\tau}{\tau_c} \sum_i \left[\frac{\sigma^+}{2} e^{-i2\pi \mathbf{R}_i \cdot (\mathbf{k} - \mathbf{h})} + \text{H.c.} \right]. \quad (\text{C21})$$

Now it is easy to evaluate Eq. (C18):

$$\mu = \lim_{\omega \rightarrow 0} \frac{2\pi}{|\omega|\tau_c} \sum_{\mathbf{R}, \mathbf{R}'} \frac{\mathbf{R} \cdot \mathbf{R}'}{D} \int \frac{d\tau}{\tau_c} (1 - e^{i\omega\tau}) t^2 \langle e^{i2\pi[\mathbf{R} \cdot \mathbf{k}(\tau) + \mathbf{R}' \cdot \mathbf{k}(0)]} \rangle \quad (\text{C22})$$

where $\langle \dots \rangle$ denotes the connected part of an average. In the small t limit, we may Taylor series-expand the above equation and write

$$t^2 \langle e^{i2\pi[\mathbf{R} \cdot \mathbf{k}(\tau) + \mathbf{R}' \cdot \mathbf{k}(0)]} \rangle = \sum_n \frac{t^{n+2}}{n!} \langle e^{i2\pi[\mathbf{R} \cdot \mathbf{k}(\tau) + \mathbf{R}' \cdot \mathbf{k}(0)]} (-S_t)^n \rangle_0 \quad (\text{C23})$$

$$= \sum_n \frac{t^{n+2}}{n!} \int \prod_{i=1}^n \left(\frac{d\tau_i}{\tau_c} \right) \sum_{\{\mathbf{R}_i\}} \langle e^{i2\pi[\mathbf{R} \cdot \mathbf{k}(\tau) + \mathbf{R}' \cdot \mathbf{k}(0) + \sum_i \mathbf{R}_i \cdot \mathbf{k}(\tau_i)]} \rangle_0, \quad (\text{C24})$$

where $\langle \dots \rangle_0$ is the connected part of an average over S_0 [Eq. (6.11)]. Note that the lattice vector is alternately chosen from $\{\mathbf{R}_i\}$ and $\{-\mathbf{R}_i\}$. The first non-vanishing term is second order in t and is given by

$$\mu^{(2)} = \lim_{\omega \rightarrow 0} \frac{2\pi t^2}{|\omega|\tau_c^2} \sum_{\mathbf{R}} \frac{|\mathbf{R}|^2}{D} \int d\tau (1 - e^{i\omega\tau}) \langle e^{i2\pi \mathbf{R} \cdot [\mathbf{k}(\tau) - \mathbf{k}(0)]} \rangle_0 \quad (\text{C25})$$

$$= \lim_{\omega \rightarrow 0} \frac{2\pi t^2}{|\omega|\tau_c^2} \int d\tau (1 - e^{i\omega\tau}) \left(\frac{\tau_c^2}{\tau^2 + \tau_c^2} \right)^{D/(D+1)} \quad (\text{C26})$$

$$= 2\pi^2 t^2 (|\omega|\tau_c)^{-2/(D+1)}. \quad (\text{C27})$$

From a similar calculation, the next order term is given by

$$\mu^{(4)} = \lim_{\omega \rightarrow 0} \frac{\pi t^4}{|\omega|\tau_c^4} \sum_{\mathbf{R}, \mathbf{R}', \mathbf{R}_1} \frac{\mathbf{R} \cdot \mathbf{R}'}{D} \int d\tau d\tau_1 d\tau_2 (1 - e^{i\omega\tau}) \langle e^{i2\pi[\mathbf{R} \cdot \mathbf{k}(\tau) + \mathbf{R}' \cdot \mathbf{k}(0) + \mathbf{R}_1 \cdot \mathbf{k}(\tau_1) - (\mathbf{R} + \mathbf{R}' + \mathbf{R}_1) \cdot \mathbf{k}(\tau_2)]} \rangle_0 \quad (\text{C28})$$

$$= - \lim_{\omega \rightarrow 0} \frac{4\pi D t^4}{|\omega|} \int' d\tau d\tau_1 d\tau_2 \frac{1}{[(\tau_2 - \tau_1)^2 + \tau_c^2] [\tau^2 + \tau_c^2]} \quad (\text{C29})$$

$$= -4\pi^2 D t^4 [1 - \ln(|\omega|\tau_c)], \quad (\text{C30})$$

where we kept only the highest order terms in D . In Eq. (C29), \int' means an integration over the range

$$\tau_1 < 0 < \tau_2 < \tau \quad \text{and} \quad 0 < \tau_1 < \tau < \tau_2. \quad (\text{C31})$$

Combining Eqs. (C27) and (C30) and writing them in terms of the renormalized tunneling amplitude t^R , the mobility is given by

$$\mu = 2\pi^2 \left[(t^R)^2 - 2D (t^R)^4 \right]. \quad (\text{C32})$$

Substituting the fixed point value t^* in Eq. (C13), the above equation becomes

$$\mu^* = 2\pi^2 \left(\frac{1}{D^2} - \frac{6}{D^3} \right) + \mathcal{O} \left(\frac{1}{D^4} \right). \quad (\text{C33})$$

When $N = D + 1$, this is consistent with the exact solution Eq. (8.38).

- ¹ *Perspectives in Quantum Hall Effects*, edited by S. D. Sarma and A. Pinczuk (Wiley, New York, 1997).
- ² S. Tarucha, T. Honda, and T. Saku, *Solid State Commun.* **94**, 413 (1995).
- ³ F. P. Milliken, C. P. Umbach, and R. A. Webb, *Solid State Commun.* **97**, 309 (1996).
- ⁴ A. M. Chang, L. N. Pfeiffer, and K. W. West, *Phys. Rev. Lett.* **77**, 2538 (1996).
- ⁵ *Single charge tunneling*, edited by H. Grabert and M. Devoret (Plenum, New York, 1992).
- ⁶ A. Furusaki and K. A. Matveev, *Phys. Rev. B* **52**, 16676 (1995).
- ⁷ This is the series conductance of two incoherent point contacts with two spin channels. For each contact, $G = 2e^2/h$.
- ⁸ L. I. Glazman and K. A. Matveev, Lifting of the Coulomb blockade of one-electron tunneling by quantum fluctuations, *Zh. Eksp. Teor. Fiz.* **98**, 1834 (1990) [*Sov. Phys. JETP* **71**, 1031 (1990)].
- ⁹ K. A. Matveev, Quantum fluctuations of the charge of a metal particle under the Coulomb blockade condition, *Zh. Eksp. Teor. Fiz.* **99**, 1598 (1991) [*Sov. Phys. JETP* **72**, 892 (1991)].
- ¹⁰ D. Berman, N. B. Zhitenev, R. C. Ashoori, and M. Shayegan, *Phys. Rev. Lett.* **82**, 161 (1999).
- ¹¹ A. Furusaki and K. A. Matveev, *Phys. Rev. Lett.* **75**, 709 (1995).
- ¹² H. Yi and C. L. Kane, *Phys. Rev. B* **57**, 5579 (1998).
- ¹³ G. Toulouse, *Phys. Rev. B* **2**, 270 (1970).
- ¹⁴ A. O. Caldeira and A. J. Leggett, *Ann. Phys. (N.Y.)* **149**, 374 (1983).
- ¹⁵ A. Schmid, *Phys. Rev. Lett.* **51**, 1506 (1983).
- ¹⁶ M. P. A. Fisher and W. Zwerger, *Phys. Rev. B* **32**, 6190 (1985).
- ¹⁷ C. L. Kane and M. P. A. Fisher, *Phys. Rev. Lett.* **68**, 1220 (1992).
- ¹⁸ C. L. Kane and M. P. A. Fisher, *Phys. Rev. B* **46**, 15233 (1992).
- ¹⁹ A. Yacoby, H. L. Stormer, N. S. Wingreen, L. N. Pfeiffer, K. W. Baldwin, and K. W. West, *Phys. Rev. Lett.* **77**, 4612 (1996).
- ²⁰ K. Moon, H. Yi, C. L. Kane, S. M. Girvin, and M. P. A. Fisher, *Phys. Rev. Lett.* **71**, 4381 (1993).
- ²¹ H. Yi and C. L. Kane, *Phys. Rev. B* **53**, 12956 (1996).
- ²² C. Nayak, M. P. A. Fisher, A. W. W. Ludwig, and H. H. Lin, *Phys. Rev. B* **59**, 15694 (1999).
- ²³ B. J. van Wees, H. van Houten, C. W. J. Beenakker, J. G. Williamson, L. P. Kouwenhoven, D. van der Marel, and C. T. Foxon, *Phys. Rev. Lett.* **60**, 848 (1988).
- ²⁴ D. A. Wharam, T. J. Thornton, R. Newbury, M. Pepper, H. Ahmed, J. E. F. Frost, D. G. Hasko, D. C. Peacock, D. A. Ritchie, and G. A. C. Jones, *J. Phys. C* **21**, L209 (1988).
- ²⁵ G. Timp, in *Mesoscopic Phenomena in Solids*, edited by B. L. Altshuler, P. A. Lee, and R. A. Webb (Elsevier, Amsterdam, 1991).
- ²⁶ R. Landauer, *Philos. Mag.* **21**, 863 (1970).
- ²⁷ K. A. Matveev, *Phys. Rev. B* **51**, 1743 (1995).
- ²⁸ For a review of the standard bosonization technique, see J. Solyom, *Adv. Phys.* **28**, 201 (1970); V. J. Emery, in *Highly Conducting One-Dimensional Solids*, edited by J. T. Devreese (Plenum, New York, 1979); J. von Delft and H. Schoeller, *Annalen der Physik*, **7**, 225 (1998); cond-mat/9805275.
- ²⁹ F. D. M. Haldane, *J. Phys. C* **14**, 2585 (1981).
- ³⁰ A. Furusaki and N. Nagaosa, *Phys. Rev. B* **47**, 4631 (1993).
- ³¹ P. Fendley, A. W. W. Ludwig, and H. Saleur, *Phys. Rev. Lett.* **74**, 3005 (1995).
- ³² V. J. Emery and S. Kivelson, *Phys. Rev. B* **46**, 10812 (1992).
- ³³ A. W. W. Ludwig and I. Affleck, *Nucl. Phys. B* **360**, 641 (1991).
- ³⁴ For a complete definition of a symmorphic lattice, see, for example, Chap. 9 in J. F. Cornwell, *Group Theory in Physics*, Vol. 1 (Academic Press, London 1984).
- ³⁵ We also get a hexagonal close-packed lattice by stacking up triangular lattices, but FCC is the only *symmorphic* lattice so obtained. Therefore, there is no ambiguity in this construction.
- ³⁶ M. Fabrizio and A. O. Gogolin, *Phys. Rev. B* **50**, 17732 (1994).
- ³⁷ P. W. Anderson, G. Yuval, and D. R. Hamann, *Phys. Rev. B* **1**, 4464 (1970).
- ³⁸ A. W. W. Ludwig and I. Affleck, *Nucl. Phys. B* **428**, 545 (1994).
- ³⁹ I. Affleck and A. W. W. Ludwig, *Phys. Rev. B* **48**, 7297 (1993).
- ⁴⁰ A similar analysis using a Monte Carlo simulation has been done for the fractional quantum Hall edge transport problem in Ref. [20].

D	lattice $\{\mathbf{R}\}$	$ \mathbf{G}_0 ^2$	dv/dl	v^*	Δ	μ^*
2	triangular	$1 + \epsilon$	$-\epsilon v + 2v^2$	$\frac{\epsilon}{2}$	$1 - \epsilon$	$1 - \frac{3\pi^2}{2}\epsilon^2$
	honeycomb	$1 - \epsilon$	$\epsilon v - 2v^2$	$\frac{\epsilon}{2}$	$1 + \epsilon$	$1 - \frac{3\pi^2}{2}\epsilon^2$
3	FCC	$1 + \epsilon$	$-\epsilon v + (A_3 + B_3)v^3$	$\sqrt{\frac{\epsilon}{A_3 + B_3}}$	$1 - 2\epsilon$	$1 - \frac{16\pi^2}{3(A_3 + B_3)}\epsilon$
	diamond	$1 - \epsilon$	$\epsilon v - (A_3 - B_3)v^3$	$\sqrt{\frac{\epsilon}{A_3 - B_3}}$	$1 + 2\epsilon$	$1 - \frac{16\pi^2}{3(A_3 - B_3)}\epsilon$
$D \geq 4$	generalized FCC	$1 + \epsilon$	$-\epsilon v + B_D v^3$	$\sqrt{\frac{\epsilon}{B_D}}$	$1 - 2\epsilon$	$1 - \frac{4(D+1)\pi^2}{DB_D}\epsilon$
	generalized diamond	$1 + \epsilon$	$-\epsilon v + B_D v^3$	$\sqrt{\frac{\epsilon}{B_D}}$	$1 - 2\epsilon$	$1 - \frac{4(D+1)\pi^2}{DB_D}\epsilon$

$A_3 = 6B(1/3, 1/3) = 6 \frac{\Gamma(1/3)\Gamma(1/3)}{\Gamma(2/3)} \approx 31.80$
 $B_D = 2D \int_0^1 dx \left[\frac{x^{2/D} + x^{-2/D} - 2}{(1-x)^2} + \left(\frac{x}{1-x}\right)^{2/D} - 1 \right], (B_3 = 4\sqrt{3}\pi \approx 21.77, B_\infty = 0)$

TABLE I. Results of the renormalization group analysis near $|\mathbf{G}_0|^2 = 1$ for small v . We assume $\epsilon > 0$. μ^* is the mobility and Δ is the scaling dimension of the most relevant operator, both at the fixed point v^* .

D	lattice $\{\mathbf{R}\}$	$ \mathbf{R}_0 ^2$	dt/dl	t^*	Δ	μ^*
2	triangular	$1 + \epsilon$	$-\epsilon t + 2t^2$	$\frac{\epsilon}{2}$	$1 - \epsilon$	$\frac{3\pi^2}{2}\epsilon^2$
	honeycomb	$1 - \epsilon$	$\epsilon t - 3t^3$	$\sqrt{\frac{\epsilon}{3}}$	$1 + 2\epsilon$	$\pi^2\epsilon$
3	FCC	$1 + \epsilon$	$-\epsilon t + 4t^2$	$\frac{\epsilon}{4}$	$1 - \epsilon$	$\frac{\pi^2}{2}\epsilon^2$
	diamond	$1 - \epsilon$	$\epsilon t - C_3 t^3$	$\sqrt{\frac{\epsilon}{C_3}}$	$1 + 2\epsilon$	$\frac{8\pi^2}{3C_3}\epsilon$
$D \geq 4$	generalized FCC	$1 + \epsilon$	$-\epsilon t + 2(D-1)t^2$	$\frac{\epsilon}{2(D-1)}$	$1 - \epsilon$	$\frac{(D+1)\pi^2}{2(D-1)^2}\epsilon^2$
	generalized diamond	$1 - \epsilon$	$\epsilon t - C_D t^3$	$\sqrt{\frac{\epsilon}{C_D}}$	$1 + 2\epsilon$	$\frac{2(D+1)\pi^2}{DC_D}\epsilon$

$C_D = D + 1 - 2 \int_0^1 dx \frac{1}{x^2} [D(1-x)^{2/D} - D + 2x], (C_2 = 3, C_\infty = D + 5 + \mathcal{O}(D^{-1}))$

TABLE II. Results of the renormalization group analysis near $|\mathbf{R}_0|^2 = 1$ for small t . We assume $\epsilon > 0$. μ^* is the mobility and Δ is the scaling dimension of the most relevant operator, both at the fixed point t^* .

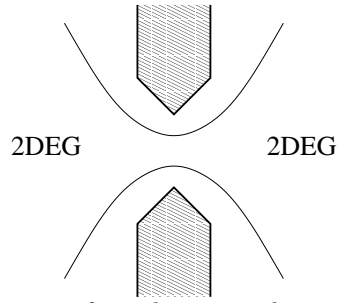


FIG. 1. Schematic view of a quantum point contact formed in a two-dimensional electron gas (2DEG). The shaded regions are metal gates and the thin lines are the boundaries of the 2DEG. Negative voltage on the gates depletes electrons underneath them and separates the 2DEG into two regions connected only by a narrow channel.

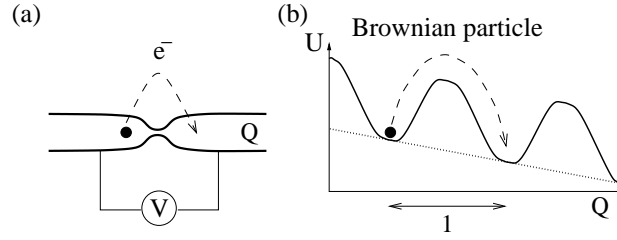


FIG. 2. Analogy between a quantum point contact and the quantum Brownian motion in a tilted periodic potential.

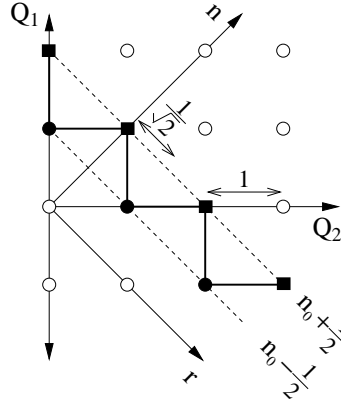


FIG. 3. Minima of the periodic potential in Q_1 - Q_2 space. After n has been integrated out, the on-resonance model is described by the corrugated 1D lattice. The two sets of degenerate sites in the lattice are depicted by filled circles and squares.

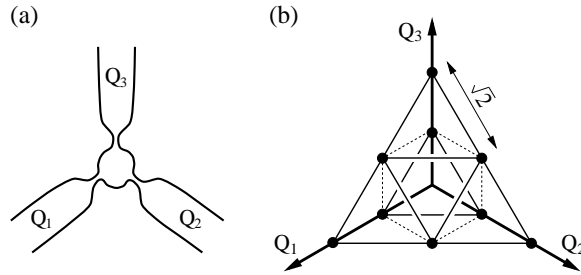


FIG. 4. (a) Schematic view of a three-lead quantum dot model. (b) Two adjacent planes of triangular lattices, or equivalently, a corrugated honeycomb lattice, which are embedded in a cubic lattice. It is a view from the (111) direction.

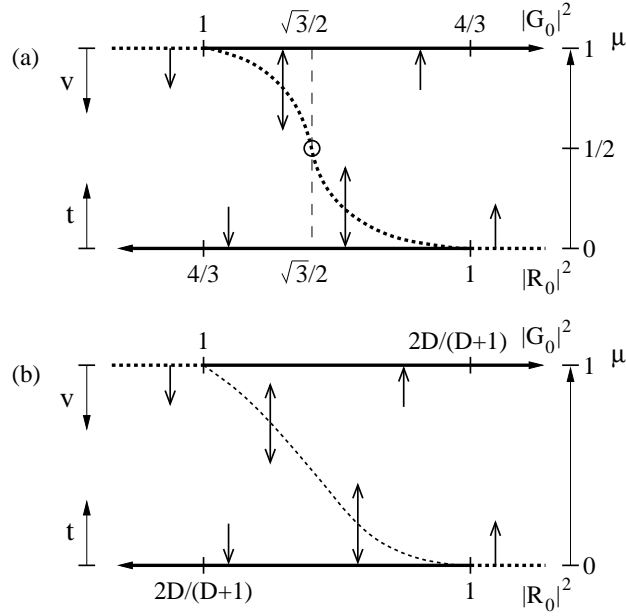


FIG. 5. Flow diagrams for symmorphic lattices: (a) triangular lattice; (b) D -dimensional generalized FCC lattice. The top (bottom) line in each diagram represents the small v (t) limit. Stable (unstable) fixed points are depicted by solid (dotted) lines, and arrows indicate the renormalization group flows. The fixed point mobility is known exactly at the self-dual point (dashed line) and perturbatively near $|G_0|^2 = 1$ and $|R_0|^2 = 1$.

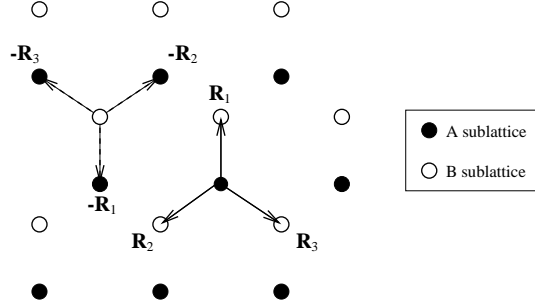


FIG. 6. Shortest displacement vectors in a honeycomb lattice.

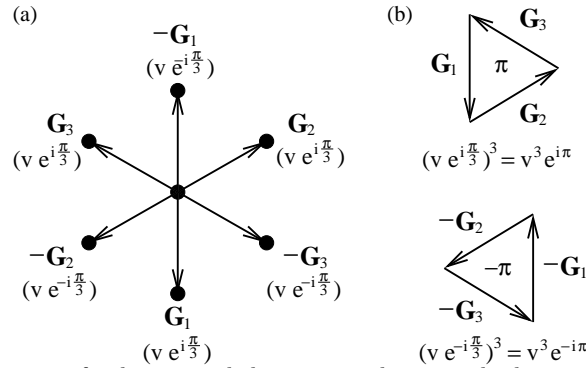


FIG. 7. (a) Reciprocal lattice vectors of a honeycomb lattice are shown with the amplitudes. (b) A phase factor $e^{\pm i\pi}$ is acquired from a trip around a triangle, which is analogous to a tight-binding model with flux $\pm\pi$ per plaquette.

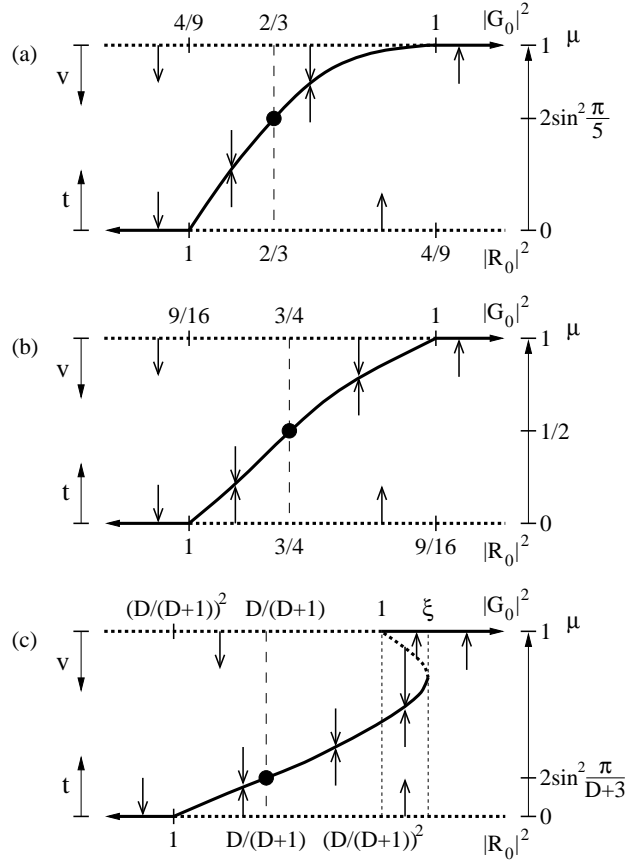


FIG. 8. Flow diagrams similar to Fig. 4 for non-symmorphic lattices – (a) honeycomb lattice, (b) diamond lattice, and (c) their generalizations to $D \geq 4$. The fixed point mobility is known exactly at the Toulouse limit (dashed lines) and perturbatively near $|\mathbf{G}_0|^2 = 1$ and $|\mathbf{R}_0|^2 = 1$.

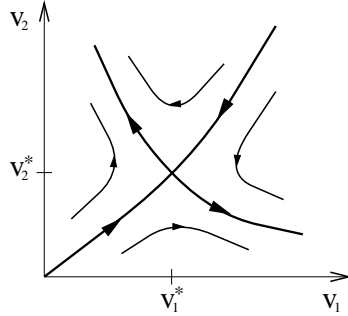


FIG. 9. Schematic diagram of renormalization group flows for the distorted honeycomb lattice model, which describes resonant tunneling of spin-1/2 Luttinger liquid [Ref. 18].

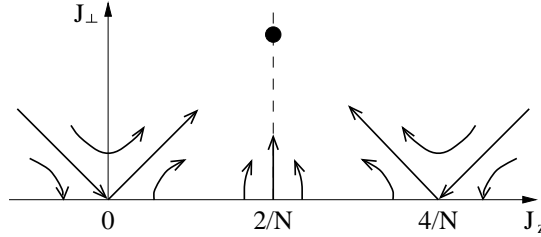


FIG. 10. Flow diagram of the N channel Kondo model for small J_\perp . The dashed line is the Toulouse limit, $J_z = 2/N$. The strong coupling fixed point is marked with the full circle.